Sel. Math. New Ser.
DOI 10.1007/s00029-017-0312-z

Selecta Mathematica
New Series

Infinitely many monotone Lagrangian tori in del Pezzo surfaces

Renato Vianna[1]

Abstract We construct almost toric fibrations (ATFs) on all del Pezzo surfaces, endowed with a monotone symplectic form. Except for $\mathbb{C}P^2\#\overline{\mathbb{C}P^2}$, $\mathbb{C}P^2\#2\overline{\mathbb{C}P^2}$, we are able to get almost toric base diagrams (ATBDs) of triangular shape and prove the existence of infinitely many symplectomorphism (in particular Hamiltonian isotopy) classes of monotone Lagrangian tori in $\mathbb{C}P^2\#k\overline{\mathbb{C}P^2}$ for $k = 0, 3, 4, 5, 6, 7, 8$. We name these tori $\Theta^{n_1,n_2,n_3}_{p,q,r}$. Using the work of Karpov-Nogin, we are able to classify all ATBDs of triangular shape. We are able to prove that $\mathbb{C}P^2\#\overline{\mathbb{C}P^2}$ also has infinitely many monotone Lagrangian tori up to symplectomorphism and we conjecture that the same holds for $\mathbb{C}P^2\#2\overline{\mathbb{C}P^2}$. Finally, the Lagrangian tori $\Theta^{n_1,n_2,n_3}_{p,q,r} \subset X$ can be seen as monotone fibres of ATFs, such that, over its edge lies a fixed anticanonical symplectic torus Σ. We argue that $\Theta^{n_1,n_2,n_3}_{p,q,r}$ give rise to infinitely many exact Lagrangian tori in $X \setminus \Sigma$, even after attaching the positive end of a symplectization to $\partial(X \setminus \Sigma)$.

Mathematics Subject Classification 53D12 · 53D05

Contents

The author is supported by the Herschel Smith postdoctoral fellowship from the University of Cambridge.

✉ Renato Vianna
r.vianna@dpmms.cam.ac.uk

[1] Centre for Mathematical Sciences, University of Cambridge, Cambridge CB3 0WB, UK

Published online: 17 February 2017

1 Introduction

We say that two Lagrangians submanifolds of a symplectic manifold X belong to the same *symplectomorphism class* if there is a symplectomorphism of X sending one Lagrangian to the other. Similar for *Hamiltonian isotopy class*.

In [37], it is explained how to get infinitely many symplectomorphism classes of monotone Lagrangian tori in $\mathbb{C}P^2$. The idea is to construct different almost toric fibrations (denoted from here by ATF) [23,31] of $\mathbb{C}P^2$. The procedure starts by applying *nodal trades* [23,31] to the corners of the moment polytope and subsequently applying a series of *nodal slides* [23,31] through the monotone fibre of the ATF. In that way we obtain infinitely many monotone Lagrangian tori $T(a^2, b^2, c^2)$ as the central fibre of some almost toric base diagram (denoted from here by ATBD) describing an ATF. They are indexed by Markov triples (a, b, c), i.e., positive integer solutions of $a^2 + b^2 + c^2 = 3abc$. We refer the reader to [37] for a detailed account.

One can see that the technique to construct ATFs and potentially get infinitely many symplectomorphism classes of monotone Lagrangian tori would also apply for any monotone toric symplectic 4-manifolds, namely $\mathbb{C}P^1 \times \mathbb{C}P^1$ and $\mathbb{C}P^2\#k\overline{\mathbb{C}P^2}$, $0 \leq k \leq 3$.

Even though we do not have a toric structure in $\mathbb{C}P^2\#k\overline{\mathbb{C}P^2}$, $3 \leq k \leq 8$ endowed with a monotone symplectic form, in this paper we show that we can actually construct ATFs in all monotone del Pezzo surfaces, i.e., $\mathbb{C}P^1 \times \mathbb{C}P^1$ and $\mathbb{C}P^2\#k\overline{\mathbb{C}P^2}$, $0 \leq k \leq 8$. Moreover, for each del Pezzo we can construct infinitely many ATFs, by applying mutations on ATBDs (Definition 2.3), and use them to describe infinitely many monotone Lagrangian tori.

In [21] and [27,28], Li–Liu and Ohta–Ono proved that the diffeomorphism type of any closed monotone symplectic 4-manifold is $\mathbb{C}P^1 \times \mathbb{C}P^1$ and $\mathbb{C}P^2\#k\overline{\mathbb{C}P^2}$, $0 \leq k \leq 8$, based on the work of McDuff [24] and Taubes [32–34]. Also, in [25], McDuff showed uniqueness of blowups (of given sizes) for 4-manifolds of non-simple Seiberg-Witten

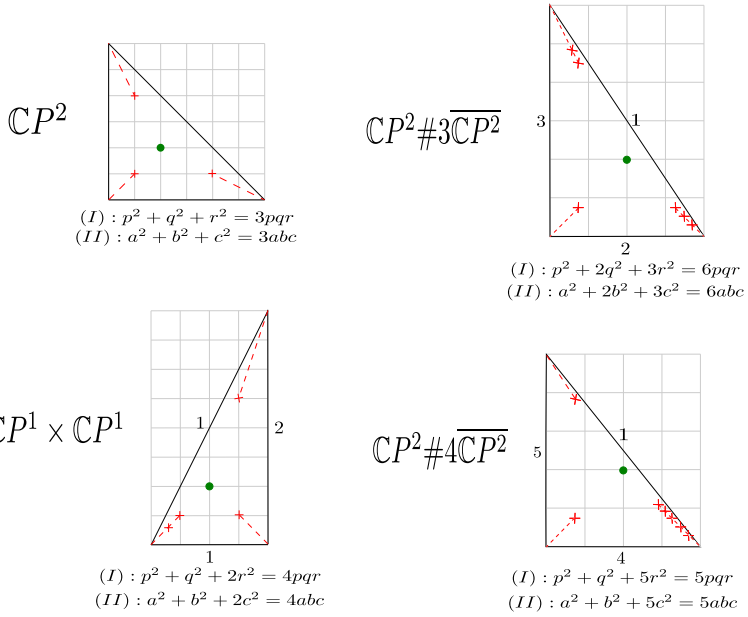

Fig. 1 ATBDs of $\mathbb{C}P^2$, $\mathbb{C}P^1 \times \mathbb{C}P^1$, $\mathbb{C}P^2\#2\overline{\mathbb{C}P^2}$, $\mathbb{C}P^2\#4\overline{\mathbb{C}P^2}$ of triangular shape

type (which includes $\mathbb{C}P^2$). Finally, from the uniqueness of the monotone symplectic form for $\mathbb{C}P^2$ and $\mathbb{C}P^1 \times \mathbb{C}P^1$ [14,24,32,34] (see also the excellent survey [29]), we get uniqueness of monotone symplectic structures on $\mathbb{C}P^1 \times \mathbb{C}P^1$ and $\mathbb{C}P^2\#k\overline{\mathbb{C}P^2}$, $0 \leq k \leq 8$. We refer the latter as del Pezzo surfaces thinking of them as endowed with a monotone symplectic form.

In Figs. 1, 2, 3 and 4, we describe several ATBDs of triangular shape (Definition 2.11), representing ATFs in del Pezzo surfaces. We refer the reader not yet familiar with ATFs to [23,31] for learning how to interpret an ATBD. In each ATBD described in this paper, the nodal fibre is represented by a '×', the dashed lines emerging from it represent cuts in the ATF and encode the monodromy around the nodal fibre. The monotone fibre is represented by a dot, and all the cuts "point towards it". We sometimes depict the affine length (Definition 2.1) of an edge of the ATBD near it. We always normalise the lattice, so that the affine lengths of the edges are pairwise coprime. We use a background grid that will help us in performing mutations (Definition 2.3) and determining the mutated eigenrays (Definition 2.12). Note that the grid often corresponds to a scaled version of the lattice we use to determine the affine lengths. Each ATBD of triangular shape is associated to integer equations called Markov type I and II equations (Definitions 2.5, 2.6, 2.13), and their meaning are explained later. For now, we just mention that the ATBDs depicted in Figs. 1, 2, 3 and 4 are associated to minimal solutions (Definition 2.9) of the corresponding Markov type I and II equations, which are written below the ATBDs. Moreover, starting from these ATBDs we can get an ATBD associated to any solution of the corresponding Markov type I (or II) equation via a series of total mutations (Definitions 2.3, 2.4).

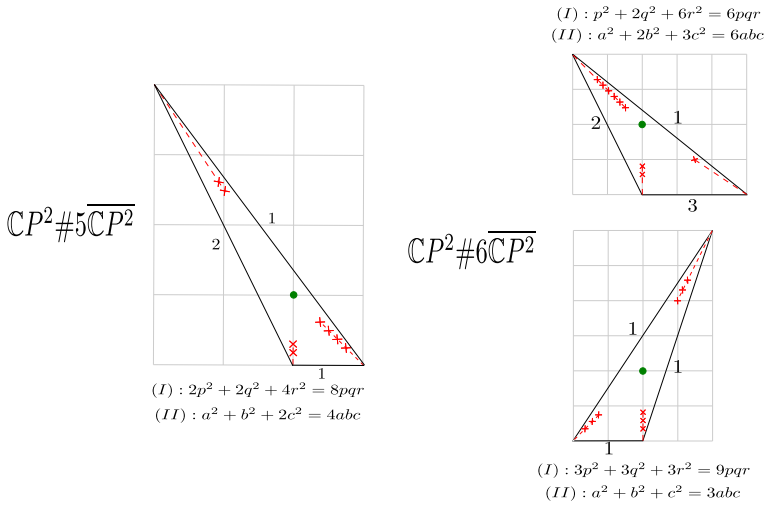

Fig. 2 ATBDs of $\mathbb{C}P^2\#5\overline{\mathbb{C}P^2}$, $\mathbb{C}P^2\#6\overline{\mathbb{C}P^2}$ of triangular shape

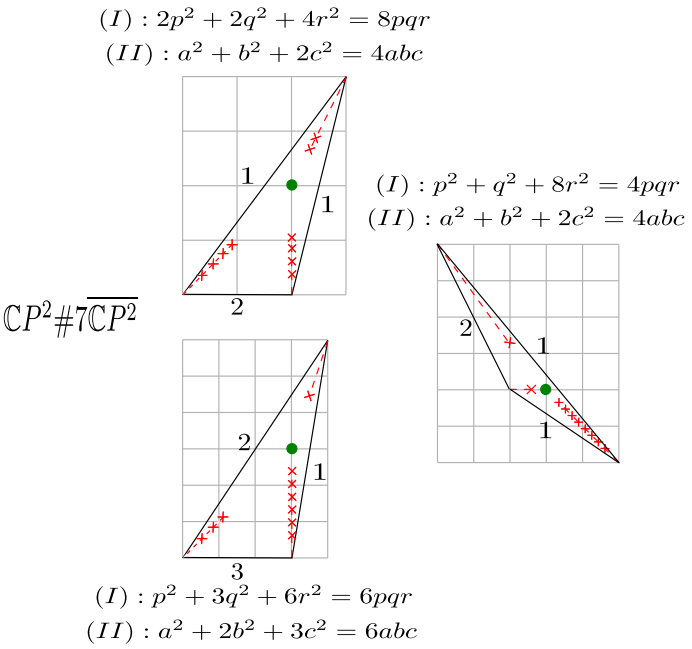

Fig. 3 ATBDs of $\mathbb{C}P^2\#7\overline{\mathbb{C}P^2}$ of triangular shape

The algebraic count of Maslov index 2 pseudo-holomorphic disks with boundary on a monotone Lagrangian L and relative homotopy class β is an invariant of the symplectomorphism class of L, first pointed out in [9]. To distinguish the monotone Lagrangian tori we built in $\mathbb{C}P^2$, we used an invariant of symplectomorphism classes of monotone Lagrangians L in the same symplectomorphism class based on the above

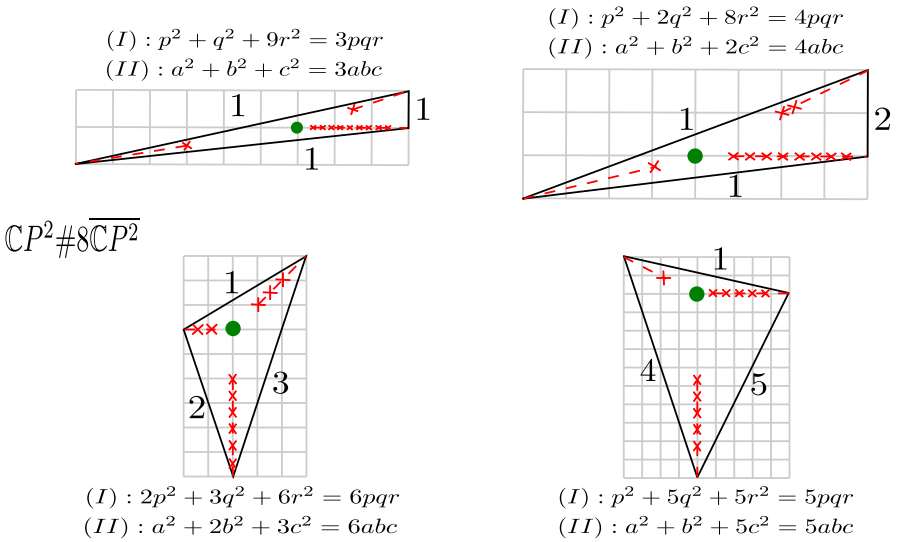

Fig. 4 ATBDs of $\mathbb{C}P^2\#8\overline{\mathbb{C}P^2}$ of triangular shape

count [37]. We named it the *boundary Maslov-2 convex hull* $\mho_L$ [37, Section 4], which is the convex hull in $H_1(L)$ of the set formed by the boundary of Maslov index 2 classes in $\pi_2(X, L)$ that have non-zero enumerative geometry. In other words, it is the convex hull for the Newton polytope of the superpotential function—for the definition of the superpotential we refer the reader to [1,2,11].

To compute the above invariant, we employed the neck-stretching technique [3,8] to get a degenerated limit of pseudo-holomorphic disks with boundary in $T(a^2, b^2, c^2)$ inside the weighted projective space $\mathbb{C}P(a^2, b^2, c^2)$. We then used positivity of intersection for orbifold disks [4,6] in the weighted projective space $\mathbb{C}P(a^2, b^2, c^2)$, together with the computation of holomorphic disks away from the orbifold points [5] to be able to compute $\mho_{T(a^2,b^2,c^2)}$, the boundary Maslov-2 convex hull for $T(a^2, b^2, c^2)$. It followed that $\mho_{T(a^2,b^2,c^2)}$ was incongruent (not related via $SL(2, \mathbb{Z})$ upon a choice of basis for the respective first homotopy groups) to $\mho_{T(d^2,e^2,f^2)}$, if $\{a, b, c\} \neq \{d, e, f\}$.

The aim of this paper is to prove:

Theorem 1.1 *There are infinitely many symplectomorphism classes of monotone Lagrangian tori inside:*

(a) $\mathbb{C}P^1 \times \mathbb{C}P^1$ *and* $\mathbb{C}P^2\#k\overline{\mathbb{C}P^2}$, $k = 0, 3, 4, 5, 6, 7, 8$;
(b) $\mathbb{C}P^2\#\overline{\mathbb{C}P^2}$;

The proof of items (a), (b) of the above theorem differ a little.

Remark 1.2 The forthcoming work of Pascaleff–Tonkonog will present a proof for the wall-crossing formula ([1,2,35], see also [15]). With that in hand, one can prove Theorem 1.1 for $\mathbb{C}P^2\#2\overline{\mathbb{C}P^2}$. Indeed, one can show that the boundary Maslov-2 convex

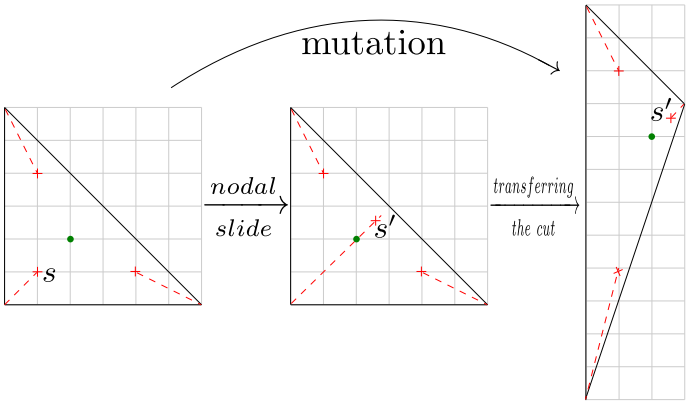

Fig. 5 We illustrate: an example of a nodal slide with respect to the node s for between ATFs of $\mathbb{C}P^2$, described by the first two ATBDs; a transferring the cut operation on the second ATBD, with respect to the node s'. The transformation from the first ATBD to the third ATBD is called a *mutation*

hull of each monotone fibre in the ATBDs described in Figs. 7 and 8 is determined by the limit orbifold (Definition 2.14), which here we can prove for ATBDs of triangular shape.

To prove Theorem 1.1(a) we show that for $\mathbb{C}P^1 \times \mathbb{C}P^1$ and $\mathbb{C}P^2 \# k\overline{\mathbb{C}P^2}$, $k = 0, 3, 4, 5, 6, 7, 8$, we can build the almost toric base diagrams of triangular shape described in Figs. 1, 2, 3 and 4.

From an ATF with a nodal fibre F_s, projecting over a node s in the base, we may modify the Lagrangian fibration by an operation called *nodal slide* defined in [31, Section 6.1], [23, Section 4.1]. In terms of ATBDs, the ATBD for the new fibration is obtained from the previous one precisely by sliding the node s in the direction of the associated cut (assuming we are taking the cut in an eigenray for the node s). Name s' the node of the new ATF. The first two ATBDs in Fig. 5 are related by a nodal slide.

In [37, Definition 2.1], we define a *transferring the cut operation* on an ATBD, with respect to a (cut associated to a) node s', which gives a different ATBD for the same ATF, see [37, Figures 1, 5]. We call a *mutation* of an ATBD with respect to a node s if we apply a *nodal slide operation* (we always slide the node to pass through the monotone fibre) together with a *transferring the cut operation*, with respect to s'.

The affine lengths of the edges of the ATBDs depicted in Figs. 1, 2, 3 and 4 are related to solutions of Markov type II equations of the form

$$k_1 a^2 + k_2 b^2 + k_3 c^2 = K k_1 k_2 k_3 abc, \quad (2.2)$$

where $a, b, c, k_1, k_2, k_3, K$ are positive integers.

We can apply a mutation $(a, b, c) \to (a' = K k_2 k_3 bc - a, b, c)$ to obtain a new solution of the same Markov type II equation.

Suppose we have an ATBD related to the Markov type II equation (2.2), for some K, k_1, k_2, k_3. We prove in Sect. 4 (Lemma 4.2) that a mutation of an ATBD with respect

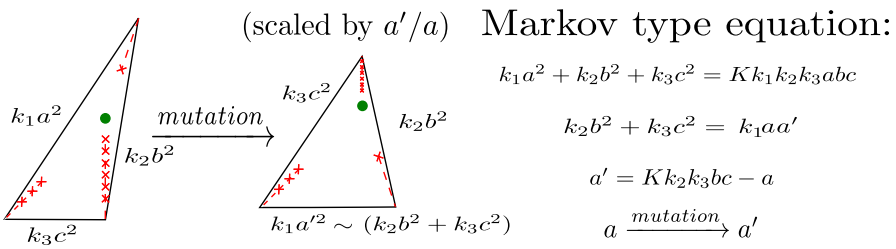

Fig. 6 Mutation of ATBD of triangular shape corresponds to mutation on Markov type II triples. The second diagram is scaled by a factor a'/a

to all nodes in the same cut corresponds to a mutation of the respective Markov type II triple solution of (2.2), as illustrated in Fig. 6.

But the affine lengths do not determine the ATBDs of triangular shape, see Fig. 3. What does is the node type (Definition 2.12). For a cut in an ATBD in the direction (m, l) (i.e. an (m, l)-eigenray—Definition 2.2), we associate a pair (n, p), where n is the number of nodes in the cut and the determinant between the primitive vectors pointing in the direction of the edges that intersect the cut have norm np^2. We say that the cut has node-type (n, p). For instance, the $(0, 1)$-eigenray in the ATBD of $\mathbb{C}P^2\#5\overline{\mathbb{C}P^2}$ depicted in Fig. 2, has two nodes and primitive vectors of the corresponding edges $(1, 0)$ and $(-1, 2)$, whose determinant is 2. Therefore, it has node-type $(2, 1)$.

An ATBD of node-type $((n_1, p), (n_2, q), (n_3, r))$ (i.e., the ATBD has three cuts with the corresponding node-type), must have (p, q, r) satisfying the Markov type I equation:

$$n_1p^2 + n_2q^2 + n_3r^2 = \sqrt{dn_1n_2n_3}pqr, \quad (2.1)$$

where p, q, r, n_1, n_2, n_3 are positive integers and $d = 12 - n_1 - n_2 - n_3$.

We name $\Theta^{n_1,n_2,n_3}_{p,q,r}$ the monotone fibre inside an ATBD of node-type $((n_1, p), (n_2, q), (n_3, r))$ (we are assuming that the fibre lives in the complement of all the cuts). We can apply the same ideas as the proof of Theorem 1.1 of [37, Section 4] to compute $\mho_{\Theta^{n_1,n_2,n_3}_{p,q,r}}$, the boundary Maslov-2 convex hull for each $\Theta^{n_1,n_2,n_3}_{p,q,r}$.

Let's call the *limit orbifold* (Definition 2.14) of an ATBD the orbifold described by the moment polytope given by deleting the cuts of the ATBD (here we assume that the cuts are all in the eigendirection of the monodromy around the respective node). Informally, we think that we nodal slide all the nodes of the ATBD towards the edge, so in the limit the described symplectic manifold by the corresponding ATF is "degenerating" to the limit orbifold.

In the proof of Theorem 1.1(a), we look at degenerated limits of pseudo-holomorphic disks with boundary in $\Theta^{n_1,n_2,n_3}_{p,q,r}$, which live in the limit orbifold of the corresponding ATBD. One important aspect we use to compute $\mho_{\Theta^{n_1,n_2,n_3}_{p,q,r}}$ is positivity of intersection between the degenerated limit of pseudo-holomorphic disks in the limit orbifold and the pre-images of the edges of the limit orbifold's moment polytope. The degenerated limit is composed by a pseudo-holomorphic disk and possibly pseudo-holomorphic spheres (the image is always connected). If it contains a multiple of a

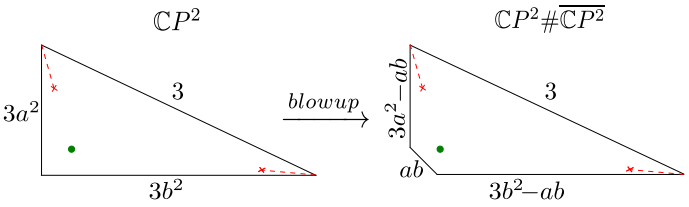

Fig. 7 ATBD of $\mathbb{C}P^2\#\overline{\mathbb{C}P^2}$ as a blowup of an ATBD of $\mathbb{C}P^2$ with affine lengths proportional to the squares of a Markov triple of the form $(1, a, b)$, with $b > a$

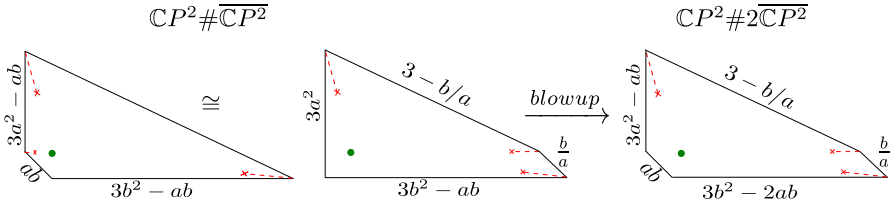

Fig. 8 ATBD of $\mathbb{C}P^2\#2\overline{\mathbb{C}P^2}$ as a blowup of an ATBD of $\mathbb{C}P^2\#\overline{\mathbb{C}P^2}$

divisor D which has negative self-intersection, it may intersect D negatively. Hence, we may loose the positivity of intersection property if the moment polytope of the limit orbifold contains an edge corresponding to a divisor with negative self-intersection, e.g. the moment polytope of the limit orbifolds of the ATBDs in Fig. 8. A divisor corresponding to an edge of the moment polytope has negative self-intersection if the sum of the angles made with the adjacent edges is bigger than π (see Remark 5.6). Therefore, a moment polytope for which all divisors corresponding to its edges have non-negative self-intersection, must be a triangle or a parallelogram.

For the cases $\mathbb{C}P^2\#k\overline{\mathbb{C}P^2}$, $k = 1, 2$, we can also construct infinitely many ATBDs, each one describing an ATF with a monotone Lagrangian torus fibre, for instance the ones in Figs. 7 and 8. Let's name $T_1(a, b)$ the monotone torus fibre of the ATF of $\mathbb{C}P^2\#\overline{\mathbb{C}P^2}$ depicted in Fig. 7, similar $T_2(a, b) \subset \mathbb{C}P^2\#2\overline{\mathbb{C}P^2}$ depicted in Fig. 8.

Even though we expect that, if $(a, b) \neq (c, d)$, there is no symplectomorphism taking $T_k(a, b)$ to $T_k(c, d)$, for $k = 1, 2$, we can't show that using our technique. That is because we loose the positivity of intersection property for the limit orbifold and hence we can't describe the boundary Maslov-2 convex hull of $T_1(a, b)$ and $T_2(a, b)$ (see Remark 1.2).

Nonetheless, for $k = 1$, we can extract enough information about the boundary Maslov-2 convex hull to show that there are infinitely many symplectomorphism classes of monotone Lagrangian tori. More precisely, we can show that $\mho_{T_1(a,b)}$ must contain a vertex with *affine angle* $b' = 3a - b$ (the norm of the determinant of the matrix formed by the primitive vectors as columns). We can also show that $\mho_{T_1(a,b)}$ is compact. Since we have infinitely many possible values for b', we must have infinitely many boundary Maslov-2 convex hulls. Therefore, Theorem 1.1(b) holds.

The following set of conjectures should be proven in the forthcoming work of Pascaleff–Tonkonog, as a result of wall-crossing, see Remark 1.2.

Conjecture 1.3 *There are infinitely many symplectomorphism classes of monotone Lagrangian tori inside* $\mathbb{C}P^2\#2\overline{\mathbb{C}P^2}$.

Consider two monotone Lagrangian fibres of ATFs whose ATBDs are related via one mutation. The algebraic count of Maslov index 2 pseudo-holomorphic disks for these tori is expected to vary according to wall-crossing formulas [1,2,15,35]. In view of that we conjecture:

Conjecture 1.4 *The boundary Maslov-2 convex hull of a monotone Lagrangian fibre of an ATF described by an ATBD (here we assume that cuts are always taken as eigenrays, which are fixed by the monodromy—see* [31, Definition 4.11]*) is determined by the limit orbifold (Definition 2.14). Actually, the vertices of the convex hull should be the primitive vectors that describe the fan of the limit orbifold.*

This would allow us to conclude:

Conjecture 1.5 *Suppose we have two monotone Lagrangian fibres of ATFs of the same symplectic manifold, described by ATBDs whose orbifold limits are different. Then they are not symplectic equivalent.*

So we expect to have many more symplectomorphism classes of monotone Lagrangian tori than the ones of $\Theta^{n_1,n_2,n_3}_{p,q,r}$, since these are the tori corresponding to ATBDs of triangular shape and, if the del Pezzo surface is not $\mathbb{C}P^2$, we should have infinitely many ATBDs not of triangular shape for which the corresponding monotone fibre would not be in the same symplectomorphism class of any torus $\Theta^{n_1,n_2,n_3}_{p,q,r}$, according to Conjecture 1.5.

Consider an ATF with no elliptic rank zero singularity [31, Definition 4.2], [35, Definition 2.7], i.e., no singular point for which the ATF is locally symplectomorphic to a corner in a toric manifold. For instance, all examples in Figs. 1, 2, 3 and 4. Call (X, ω) the corresponding symplectic manifold. The absence of elliptic rank zero singularity implies there is a smooth symplectic torus Σ living over the boundary of the base of the corresponding ATF (which projects over the edges of the ATBD) and representing the anti-canonical class [31, Proposition 8.2]. By only sliding the nodes away from a neighbourhood of Σ, we can assume that this neighbourhood remains invariant under the mutations of the ATBD's, so Σ is always living over the boundary of the base of corresponding ATF.

Assume now X is a del Pezzo surface. All the tori obtained via mutation from an starting monotone torus in X, in particular, all the tori $\Theta^{n_1,n_2,n_3}_{p,q,r} \subset X$ live on $X \setminus \Sigma$ and are in different Hamiltonian isotopy classes there. The complement of a neighbourhood $\mathcal{N}$ of Σ (specifically chosen in Sect. 5.3, e.g. in Fig. 9, $\mathcal{N}$ is the pre-image of the shaded region depicted in the first ATBD) has a contact type boundary V with a Liouville vector field pointing outside. We can actually set it up so that the orbits of the Reeb vector field in V are collapsing cycles for Σ—with respect to the toric structure in the neighbourhood of Σ.

Hence, we can attach the positive half of a symplectization, obtaining $(X \setminus \mathcal{N}) \cup (V \times [0, +\infty))$ (endowed with the corresponding symplectic form ω_∞). Note that $((X \setminus \mathcal{N}) \cup (V \times [0, C]), \omega_C)$, corresponds to a dilation of the initial ATBD and,

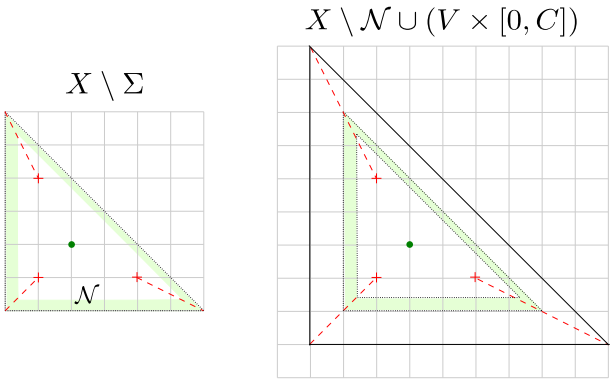

Fig. 9 For $X = \mathbb{C}P^2$, the left picture is an ATBD in $X \setminus \Sigma$. The *right picture* is the ATBD corresponding to the induced ATF in $((X \setminus \mathcal{N}) \cup (V \times [0, C]), \omega_C)$. The pre-image of the *shaded region* is the neighbourhood $\mathcal{N}$ of Σ

also, an inflation with respect to Σ [22, Section 2]—see Fig. 9. In the case that X is monotone, Σ is Poincaré dual to a multiple of the symplectic form, and hence $[\omega_C]$ is a multiple of $[\omega]$. It follows that:

Theorem 1.6 *Let X be a del Pezzo surface and Σ a smooth anti-canonical divisor and $\mathcal{N}$ its neighbourhood as above. The tori $\Theta^{n_1,n_2,n_3}_{p,q,r} \subset (X \setminus \mathcal{N}) \cup (V \times [0, +\infty))$ belong to mutually different Hamiltonian isotopy classes.*

By looking at a Lagrangian skeleton of $X \setminus \Sigma$, Shende et al. [30] can show that there exist infinitely many distinct subcategories of the category of microlocal sheaves on the Lagrangian skeleton. The Lagrangian skeleton is given by attaching Lagrangian disks to a torus. The subcategories mentioned above correspond to sheaves on the tori given by mutations that are equivalent to the ones we see in ATBDs, see Sect. 6.1.

The rest of the paper is organised as follows:

We start by defining some terminology in Sect. 2. We suggest the reader familiar with almost toric fibrations move directly to Sect. 3. In Sects. 2.2, 2.3 and 2.4, we review the notions of monotonicity, blowups and almost toric blowups as well as how to perform mutations. We recommend the reader to use Sect. 2.1 only if some terminology is not clear from the context.

In Sect. 3, we describe how to obtain all the ATBDs of Figs. 1, 2, 3 and 4, also showing how to "create space" to perform a blowup by changing the ATF. We believe that the reader should become easily acquainted with the operations on the ATBDs and be able to deduce the moves just by looking at Figs. 16, 17, 18, 19, 20 and 21. Nonetheless, we provide explicit description of each operation on the ATBDs.

In Sect. 4, we show that mutations of Markov type I and II equations correspond to mutations of ATBDs of triangular shape. We also show that any monotone ATBD of triangular shape is node-related (Definition 2.13) to a Markov type I equation. It follows from [20, Section 3.5] that Figs. 1, 2, 3 and 4 provide a complete list of ATBDs of triangular shape for del Pezzo surfaces.

In Sect. 5, we compute the boundary Maslov-2 convex hull $\mho_{\Theta_{p,q,r}^{n_1,n_2,n_3}}$ (Theorem 5.2), which finishes the proof of Theorem 1.1(a). We prove Theorem 1.1(b) in Sect. 5.2 and Theorem 1.6 in Sect. 5.3

In Sect. 6 we relate our work with [30], by pointing out that the complement of the symplectic torus Σ in the anti-canonical class is obtained from attaching (Weinstein handles along the boundary of) Lagrangian disks to the (co-disk bundle of the) monotone fibre of each ATBD. In particular, these tori are exact in the complement of Σ. We also relate our work with [18], where Keating shows how modality 1 Milnor fibres $\mathcal{T}_{p,q,r}$, for $(p,q,r) \in \{(3,3,3),(2,4,4),(2,3,6)\}$ compactify to del Pezzo surfaces of degree $d = 3,2,1$. It follows from Theorem 1.6 that there are infinitely many Hamiltonian isotopy classes of exact tori in $\mathcal{T}_{p,q,r}$, for $(p,q,r) \in \{(3,3,3),(2,4,4),(2,3,6)\}$. Also, in [17, Section 7.4], Keating mentions that all Milnor fibres $\mathcal{T}_{p,q,r}$ are obtained by attaching Lagrangian discs to a Lagrangian torus as described in [30, Example 6.3]. We conjecture then that there are infinitely many exact tori in $\mathcal{T}_{p,q,r}$ (see also [30, Example 6.3]). In Sect. 6.3, we point out that the Markov type I equations have appeared before, in relation to 3-blocks exceptional collections in the del Pezzo surfaces [20] and $\mathbb{Q}$-Gorenstein smoothing of weighted projective spaces to del Pezzo surfaces [16]. We ask if there is a correspondence between ATBDs, 3-blocks exceptional collections and $\mathbb{Q}$-Gorenstein degenerations of a given del Pezzo surface (see Questions 6.2, 6.3). Finally, we relate the ATBD of $\mathbb{C}P^1 \times \mathbb{C}P^1$ in Fig. 1 with the singular Lagrangian fibration given by Fukaya et al. [13], as well as a similar ATBD of $\mathbb{C}P^2$ with the singular Lagrangian fibration described in [38]. In [12,13] it was shown that there are a continuous of non-displaceable fibres in the monotone $\mathbb{C}P^1 \times \mathbb{C}P^1$; in $\mathbb{C}P^2 \# 2\overline{\mathbb{C}P^2}$ for blowups of sizes $(\alpha, \frac{1-\alpha}{2})$, for $\alpha > 1/3$, hence not monotone (here we take the area of the class of the line coming from $\mathbb{C}P^2$ to be 1); same for $\mathbb{C}P^2 \# k\overline{\mathbb{C}P^2}$, with blowups taken of sizes $(\alpha, \frac{1-\alpha}{2}, \epsilon_i)$; $i = 1,\dots,k-2$, with ϵ_i small enough for all $i = 1,\dots,k-2$. We ask what ATBDs have a continuous of non-displaceable fibres. In [36], a similar result is proven for the monotone $\mathbb{C}P^2 \# 3\overline{\mathbb{C}P^2}$, and for some family of tori in the monotone $(\mathbb{C}P^1)^{2m}$.

2 Terminology and background

In this section we set some terminology and review some aspects of almost toric fibrations and blowup in the symplectic category. For the definition of ATF we refer the reader to [31, Definition 4.5], [23, Definition 2.2], [35, Definition 2.7]. More details about ATFs can be found in the above references.

2.1 Terminology

Before we describe how to get almost toric fibrations on all del Pezzo surfaces, let's fix some terminology. A lot of the terminology can be intuitively grasped, so we suggest the reader to move on to the next section and only use this section as a reference for terminology.

We recall that a *primitive vector* on the standard lattice of $\mathbb{R}^2$ is an integer vector that is not a positive multiple of another integer vector.

Definition 2.1 If $v \in \mathbb{R}^2$, $w \in \mathbb{Z}^2$, $v = pw$ where w is a primitive vector and $p \in \mathbb{R}$, we say that $|p|$ is the affine length of v.

We also recall ([31, Section 5.2]) that an ATBD is the image of an affine map from the base of an ATF, minus a set of cuts, to $\mathbb{R}^2$ endowed with the standard affine structure. Let s be a node of an ATF and R^+ an eigenray ([31, Definition 4.11]) leaving s. Suppose we have an ATBD where the cut associated to s is a ray equals to "the image of" R^+.

Definition 2.2 We say that R^+ is an (m, n)-eigenray of an ATBD if it points towards the node in the direction of the primitive vector $(m, n) \in \mathbb{Z}^2 \subset \mathbb{R}^2$. We also say that s is an (m, n)-node of the ATBD.

We refer the reader to [37, Definition 2.1] for the definition of a *transferring the cut* operation with respect to an eigenray R^+. It is illustrated in the last three diagrams of Fig. 10 and the last two diagrams of Fig. 11. It essentially changes the direction of a cut in an ATBD, giving rise to another ATBD representing the same ATF. In this paper we overlook the fact that we have two options (e.g., apply the appropriate monodromy to either parts of the third diagram in Fig. 10 or the second diagram in Fig. 11) for performing a transferring the cut operation, since the two resulting ATBD are related via $SL(2, \mathbb{Z})$. The following notion of mutation is explained in Sect. 2.2.

Definition 2.3 We call a *mutation* with respect to a (m, n)-*node* an operation on an ATBD containing a monotone fibre consisting of: a nodal slide [31, Section 6.1] of the corresponding (m, n)-eigenray passing through the monotone fibre; and one transferring the cut operation with respect to the same eigenray.

Definition 2.4 A *total mutation* is a mutation with respect to all (m, n)-nodes, for some (m, n).

Definition 2.5 A Markov type I equation, is an integer equation for a triple (p, q, r) of the form:

$$n_1 p^2 + n_2 q^2 + n_3 r^2 = \sqrt{d n_1 n_2 n_3}\, pqr, \tag{2.1}$$

for some constants $n_1, n_2, n_3 \in \mathbb{Z}_{>0}$, $d = 12 - n_1 - n_2 - n_3$, so that $d n_i n_j \equiv 0 \mod n_k$, $\{i, j, k\} = \{1, 2, 3\}$ and $d n_1 n_2 n_3$ is a square. A solution (p, q, r) is called a Markov type I triple, if $p, q, r \in \mathbb{Z}_{>0}$.

Definition 2.6 Let (p, q, r) be a Markov type I triple. The Markov type I triple $(p' = \sqrt{\frac{d n_2 n_3}{n_1}} qr - p, q, r)$ is said to be obtained from (p, q, r) via a mutation with respect to p. Analogous for mutation with respect to q and r.

Definition 2.7 A Markov type II equation, is an integer equation for a triple (a, b, c) of the form:

$$k_1 a^2 + k_2 b^2 + k_3 c^2 = K k_1 k_2 k_3 abc, \tag{2.2}$$

for some constants $K, k_1, k_2, k_3 \in \mathbb{Z}_{>0}$. A solution (a, b, c) is called a Markov type II triple, if $a, b, c \in \mathbb{Z}_{>0}$.

Definition 2.8 Let (a, b, c) be a Markov type II triple. The Markov type II triple $(a' = Kk_2k_3bc - a, b, c)$ is said to be obtained from (a, b, c) via a mutation with respect to a. Analogous for mutation with respect to b and c.

Definition 2.9 A Markov type I, respectively II, triple (p, q, r), respectively (a, b, c), is said to be minimal if it minimizes the sum $p+q+r$, respectively $a+b+c$, among Markov type I, respectively II, triples.

Definition 2.10 An ATBD of triangular shape is an ATBD whose cuts are all in the direction of the respective eigenrays of the associated node and whose closure is a triangle in $\mathbb{R}^2$.

Definition 2.11 An ATBD of *length type* (A, B, C) is an ATBD of triangular shape whose edges have affine lengths *proportional* to (A, B, C).

Definition 2.12 An ATBD of *node type* $((n_1, p), (n_2, q), (n_3, r))$, is an ATBD of triangular shape with the three cuts R_1, R_2, R_3 containing respectively n_1, n_2, n_3 nodes. Moreover, the determinant of primitive vectors of the edges connecting at the cut R_1, respectively R_2, R_3, have norm equals to n_1p^2, respectively, n_2q^2, n_3r^2.

Note that the above definition can be generalised to any ATBD whose cuts are all in the direction of an eigenray leaving the respective node.

Definition 2.13 We say that an ATBD is length-related to a Markov type II equation (2.2) if it is of length type (k_1a^2, k_2b^2, k_3c^2), for some Markov type II triple (a, b, c). We say that an ATBD is node-related to a Markov type I equation (2.1) if it is of node type $((n_1, p), (n_2, q), (n_3, r))$, for some Markov type I triple (p, q, r). The total space of the corresponding ATF is a del Pezzo of degree d, i.e., for $\mathbb{C}P^2\#k\overline{\mathbb{C}P^2}$, $d = 9 - k = 12 - n_1 - n_2 - n_3$ [31, Section 8.1], and for $\mathbb{C}P^1 \times \mathbb{C}P^1$, $d = 8$.

We also define the limit orbifold of an ATBD:

Definition 2.14 Given an ATBD, its *limit orbifold* is the orbifold for which the moment map image is equal to the ATBD without the nodes and cuts, which are replaced by corners (usually not smooth). (Here we assume that cuts are always taken as eigenrays, which are fixed by the monodromy—see [31, Definition 4.11].)

2.2 Short review of mutations

In this section we give a short review of how to perform a mutation of an ATBD. Essentially we need to: slice the ATBD with respect to the eigenline ([31, Definition 4.11]) associated to the node(s) we want to mutate, dividing it in two parts; apply to either of the parts the inverse of the corresponding monodromy associated to the node(s), accordingly.

In Fig. 10 we illustrate a total mutation (Definition 2.4) with respect to the $(1, 0)$-nodes on an ATBD of $\mathbb{C}P^2\#5\overline{\mathbb{C}P^2}$ (see also Fig. 18). Often one can read of the result of a total mutation without having to make any computation regarding the monodromy. One only needs to notice that: a total mutation with respect to (m, n)-nodes aligns the edges that were bent by the monodromy encoded by the (m, n)-eigenray (Definition 2.2); it preserves affine length; and it preserves the eigendirection (m, n).

For instance, in Fig. 10, after applying the inverse of the monodromy to the top half of the third picture, we know that the mutation will align the $(2, 1)$-edge with the $(0, 1)$-edge. It preserves the affine length of the edge, which is three according to the grid. This determines the image of the top triangle of the third picture after the mutation, since the $(1, 0)$ direction is invariant. It also determines the new direction after mutation of the $(0, -1)$-eigenray, which will always point to the monotone fibre.

If the mutation is not total, one needs to take into account the monodromy. In Fig. 11, we mutate only one $(0, 1)$-node (see also Fig. 21). After cutting vertically the first ATBD in two, we apply the monodromy $\begin{bmatrix} 1 & 0 \\ 1 & 1 \end{bmatrix}^{-1} = \begin{bmatrix} 1 & 0 \\ -1 & 1 \end{bmatrix}$ (see Eq. 4.1) to the right triangle. We see the monodromy sends $\begin{bmatrix} 1 \\ 3 \end{bmatrix}$ to $\begin{bmatrix} 1 \\ 2 \end{bmatrix}$ and it preserves the affine length (three) of this edge. Since the $(0, 1)$ direction is invariant, we completely determine the image of the rightmost triangle of the middle picture in Fig. 11 after mutation. Again, the new direction of the $(-1, -1)$-eigenray is determined by the fact that it points towards the monotone fibre.

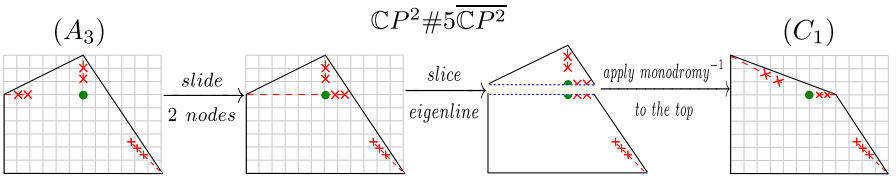

Fig. 10 Total mutation with respect to the $(1, 0)$-nodes of an ATBD of $\mathbb{C}P^2\#5\overline{\mathbb{C}P^2}$

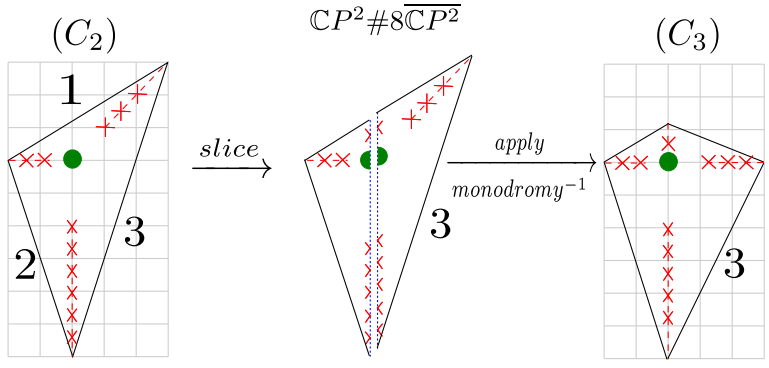

Fig. 11 A mutation with respect to one $(1, 0)$-node of an ATBD of $\mathbb{C}P^2\#8\overline{\mathbb{C}P^2}$

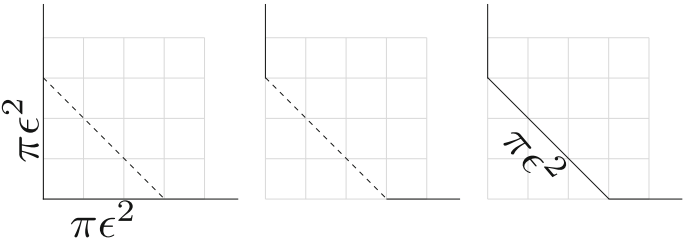

Fig. 12 Blowup of a ball $B(\epsilon)$ centered at a rank 0 singularity in a toric manifold

2.3 Monotonicity and blowup

To perform a blowup in the symplectic category [26], one deletes a symplectic ball $B(\epsilon)$ of radius ϵ and collapses the fibres of the Hopf fibration of $\partial B(\epsilon)$ to points. In particular, the blowup depends on the radius ϵ one takes. In a toric symplectic manifold, one can perform a blowup near an elliptic rank zero singularity ([31, Definition 4.2], [35, Definition 2.7]) and remain toric, provided one chooses a small enough ball compatible with the toric fibration, see Fig. 12.

We recall that a symplectic manifold (X, ω) is said to be monotone if there exists $C > 0$ such that $\forall H \in \pi_2(X)$:

$$\int_H \omega = C\mathrm{c}_1(H). \tag{2.3}$$

And Lagrangian $L \subset X$ is said to be monotone if there exists $C_L > 0$ such that $\forall \beta \in \pi_2(X, L)$:

$$\int_\beta \omega = C_L \mu_L(\beta), \tag{2.4}$$

where μ_L is the Maslov index.

Since $\mathrm{c}_1 = 2\mu_{L|\pi_2(X)}$, if $\pi_2(X) \neq 0$, then $2C = C_L$. Also, if L is orientable $\mu_L(\beta) \in 2\mathbb{Z}$.

The monotonicity condition is then affected by the size of the symplectic blow up. In dimension 4, when we perform a symplectic blowup, we modify the second homology group by adding a spherical class—coming from the quotient of S^3 under the Hopf fibration—of Chern number 1. Therefore to keep monotonicity one must choose the radius of the symplectic ball, so that the quotient sphere, also known as exceptional divisor, has the appropriate symplectic area, see Eq. (2.3).

2.4 Almost toric blowup

The following notion of *almost toric blowup* was known to Mark Gross for some time, but he told the author that he does not recall writing it. It was well described in [31, Section 5.4] and [23, Section 4.2] and it was observed before by Zung [39, Example 4.16]. The author found this notion also written in [2, Example 3.1.2], and our

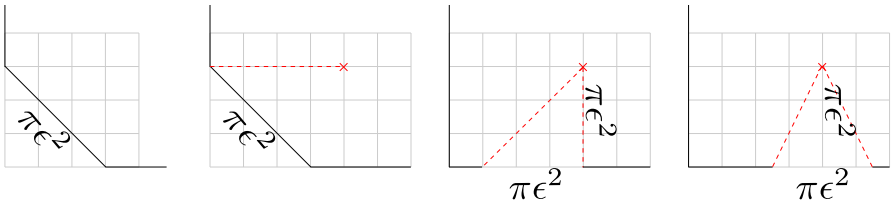

Fig. 13 ATBDs on a toric blowup

exposition relies on this example. We will perform a blowup on a point in lying over an elliptic rank one singularity ([31, Definition 4.2], [35, Definition 2.7]) of an ATF, and obtain another ATF, which agrees with the previous one away from a neighbourhood of the exceptional divisor.

We first point out that, after a toric blowup (see the first ATBD of Fig. 13), we may apply a nodal trade and get an ATF represented by the second ATBD of Fig. 13. Now we can get different ATBDs representing the same ATF, by performing cuts in different directions. If we take a cut whose direction is not in an eigendirection, this direction will not remain invariant under the monodromy. Hence in the ATBD it will be represented by two dashed segments (recall the an ATBD is an affine map to $\mathbb{R}^2$ from the *complement* of the cuts). We will abuse terminology by also saying that we are "transferring the cut" when we apply these type of branch moves [31, Section 5.3], such as from the second ATBD to the third, or forth, ATBD in Fig. 13. Note that these branch moves are not in the framework of [37, Definition 2.1].

To get from the second ATBD to the third ATBD of Fig. 13, first we slice the second ATBD of Fig. 13 by rays *leaving the node* in directions $(-1, 0)$ and $(0, -1)$, obtaining two parts; then, to the compact part, we apply the monodromy associated with the $(1, 0)$-node, $\begin{bmatrix} 1 & 1 \\ 0 & 1 \end{bmatrix}$. Note that the monodromy takes the $(0, 1)$ dashed ray in the third ATBD of Fig. 13 to the $(1, 1)$ dashed ray, that together represent the same cut in the ATF. This ATF is represented by the second, third and forth ATBDs. To get to the third ATBD in Fig. 13, we slice the second ATBD of Fig. 13 by rays *leaving the node* in directions $(-1, 0)$ and $(1, -2)$; then we proceed as before. Later we will perform these "transferring the cut operations" after an almost toric blowup, e.g., from ATBDs (A_1) to (A_2) and (D_1) to (D_2) in Figs. 20 and 21.

The above discussion makes us think that we can get the third and forth ATBDs of Fig. 13, by applying a blowup on a point over the edge of the standard moment polytope of $\mathbb{C}^2$. And indeed we can ([31, Section 5.4], [23, Section 4.2]). In [2, Example 3.1.2], Auroux show how to construct an almost toric fibration on the blowup of $\mathbb{C}^2$ over the point $(1, 0)$, which lies on the edge of the standard moment polytope of $\mathbb{C}^2$. We can than use this almost toric fibration given on the neighbourhood of the exceptional divisor as a local model for what we call *almost toric blowup*. The following proposition is an immediate consequence of [2, Example 3.1.2].

Proposition 2.15 (Gross, [39] (Example 4.16), [31] (Section 5.4), [2] (Example 3.1.2)) *Consider the blowup at* $(a, 0) \subset \mathbb{C}^2$*, with symplectic form* ω_ϵ*, with respect to the standard ball of radius* ϵ*. There is an ATF on the blowup, with one nodal singularity. Its monodromy's eigendirection is* $(1, 0)$*, i.e, parallel to the edge in the standard moment polytope of* $\mathbb{C}^2$ *containing the image of* $(a, 0)$*.*

Note that in [2, Example 3.1.2], the exceptional divisor lives over the cut in the base of the ATF, which is represented by the two dashed lines in ATBD given in [2, Figure 2]. Let $\mathcal{N}$ be a neighbourhood of the exceptional divisor, that we can identify with the pre-image of a neighbourhood of the dashed lines in [2, Figure 2], which is depicted in the second diagram of Fig. 14.

Proposition 2.16 *In $\mathbb{C}^2\#\bar{\mathbb{C}P}^2 \setminus \mathcal{N}$, the ATF of Proposition 2.15 can be made to agree with the toric one of $\mathbb{C}^2$ outside some neighbourhood $\hat{\mathcal{N}}$ of $(a, 0)$.*

Proof This follows from the fact that the symplectic form ω_ϵ agrees with the standard symplectic for of $\mathbb{C}^2$ outside a neighbourhood of the ball of radius ϵ centred at $(a, 0)$. In that region, the tori $L_{r,\lambda}$ described by Auroux in [2, Example 3.1.2] coincide with the standard product torus in $\mathbb{C}^2$, i.e., so outside some neighbourhoods $\mathcal{N} \subset \mathbb{C}^2\#\bar{\mathbb{C}P}^2$ and $\hat{\mathcal{N}} \subset \mathbb{C}^2$, the fibres of the ATF of the blowup are identified with the fibres of the standard moment polytope of $\mathbb{C}^2$. □

Consider an edge of an ATBD. Up to acting by an element of $SL(2, \mathbb{Z})$, we may assume the edge's direction is $(1, 0)$. Consider a segment $R = \pi\epsilon^2\mathbf{w}$ leaving the edge of the ATBD, where $\mathbf{w}$ is a primitive vector. For $S = \begin{bmatrix} 1 & -1 \\ 0 & 1 \end{bmatrix} R$, $R - S$ is a multiple of $(1, 0)$ (see Fig. 15); assume that the closed triangular region bounded by R, $-S$ and the edge (here, the tail of $-S$ is assumed to be at the head of R) does not intersect any cut of the ATBD and is contained inside it—as in Fig. 15; let $\bar{p}$ be the middle point between the tail of R and the head of $-S$; consider a rank one elliptic singularity p of an ATF, lying over $\bar{p}$.

Essentially what the above Propositions 2.15, 2.16 tell us is:

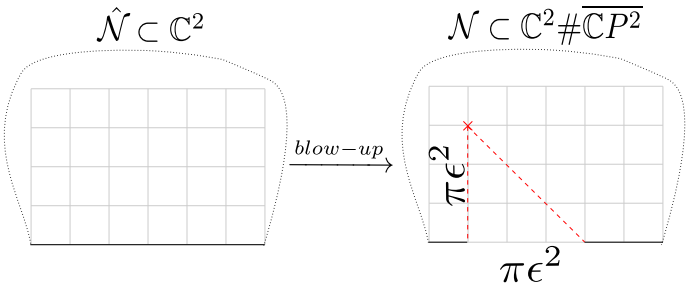

Fig. 14 Almost toric blowup

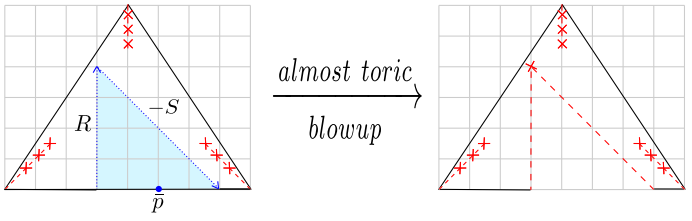

Fig. 15 Almost toric blowup

Proposition 2.17 (Gross, [39] (Example 4.16), [31] (Section 5.4)) *There is an ATF on the ϵ-blowup at the point p, with an ATBD given by replacing the region of the base bounded by the segments R, $-S$ and the edge, by cuts over R and S and a node in their intersection point.*

Definition 2.18 ([31] (Section 5.4), [23] (Section 4.2)) We say that the ATBD on the blowup described in Proposition 2.17, is obtained from the previous one via a blowup of length $\pi\epsilon^2$.

3 Almost toric fibrations of del Pezzo surfaces

One is able to perform symplectic blowup (Sect. 2.3) in one, two or three corners of the moment polytope of $\mathbb{C}P^2$ to obtain monotone toric structures on $\mathbb{C}P^2\#\overline{\mathbb{C}P^2}$, $\mathbb{C}P^2\#2\overline{\mathbb{C}P^2}$, $\mathbb{C}P^2\#3\overline{\mathbb{C}P^2}$. But one cannot go further, since it is not possible to torically embed a ball centred in a corner of the moment polytope of $\mathbb{C}P^2\#3\overline{\mathbb{C}P^2}$ and with the appropriate radius to remain monotone. (See moment polytope (A_1) in Fig. 16).

Nonetheless, it is possible to create some space for the blowup if we only require to remain almost toric.

We are now ready to describe ATFs for all del Pezzo surfaces. In all ATBDs appearing on Figs. 16, 17, 18, 19, 20, 21 and 22, the interior dot represents the monotone fibre, which we can keep track of while performing mutations (see Figs. 10, 11). Alternatively, one can use the affine structure to measure the symplectic area of disks leaving the torus fibre towards an edge and projecting into a line in the ATBD [31, Section 7.2]. They all have Maslov index two, since the anti-canonical divisor given by the pre-image of the edges of the ATBD [31, Section 8.2], seen as a cycle in the second homology of the space relative to the torus fibre, is Poincaré dual to half of the Maslov class.

The reader should easily become familiar with the operations and be able to read them from the pictures. Nonetheless, we give explicit descriptions of the operations in each step. We display below the ATBDs of triangular shape the Markov type I, respectively II, equations that are node-related, respectively length-related, to them. The importance of this relationship is explained in Sect. 4.

Remark 3.1 In this section we often change grid sizes, so it becomes easier to perform mutations and almost toric blowups.

3.1 ATFs of $\mathbb{C}P^2\#3\overline{\mathbb{C}P^2}$

To arrive at an ATF of $\mathbb{C}P^2\#4\overline{\mathbb{C}P^2}$, we perform some sequence of nodal trades and mutations on the ATBDs of $\mathbb{C}P^2\#3\overline{\mathbb{C}P^2}$ described on Fig. 16. And eventually we are able to perform a blowup, and obtain an ATBD for $\mathbb{C}P^2\#4\overline{\mathbb{C}P^2}$. We are also able to get the ATBD of triangular shape for $\mathbb{C}P^2\#3\overline{\mathbb{C}P^2}$ (Fig. 16(A_1)) appearing in Fig. 1. The operations relating each diagram in Fig. 16 are described below:

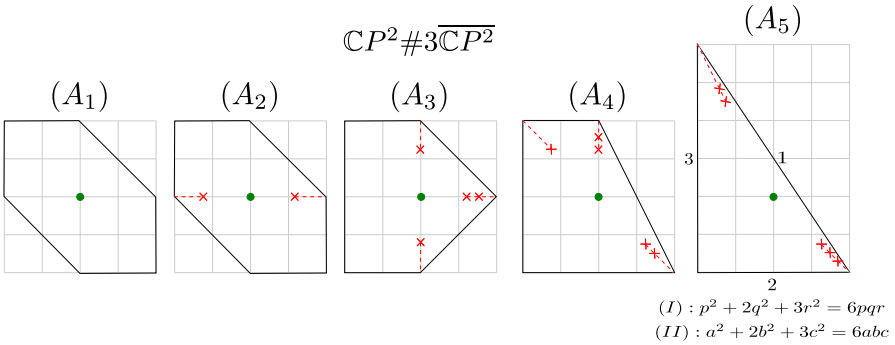

Fig. 16 ATBDs of $\mathbb{C}P^2\#3\overline{\mathbb{C}P^2}$

(A_1) Toric moment polytope for $\mathbb{C}P^2\#3\overline{\mathbb{C}P^2}$;
(A_2) Applied two nodal trades, getting $(1,0)$ and $(-1,0)$ nodes;
(A_3) Mutated $(1,0)$-node and applied two nodal trades, getting $(0,1)$ and $(0,-1)$ nodes;
(A_4) Mutated $(0,1)$-node and applied one nodal trade, getting a $(1,-1)$-node;
(A_5) Mutated $(1,-1)$-node.

We abuse the node type Definition 2.12 and assume each smooth corner of an ATBD has "node type $(1,1)$". This way the ATBD (A_5) of node type $((1,1),(2,1),(3,1))$. The same apply for ATBD (A_4) in Fig. 17 and ATBD (A_3) in Fig. 22.

3.2 ATFs of $\mathbb{C}P^2\#4\overline{\mathbb{C}P^2}$

We now see that we have created enough space to perform a toric blowup on the corner (rank 0 singularity) of the 4th or 5th ATBD of Fig. 16, in order to obtain an ATF of $\mathbb{C}P^2\#4\overline{\mathbb{C}P^2}$. We then perform some nodal trades and mutations to, not only create more space for performing another blowup, but also to get the ATBD of triangular shape in Fig. 1.

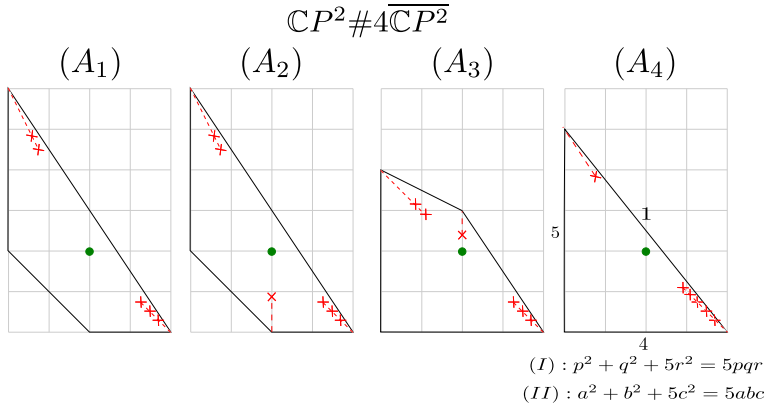

Fig. 17 ATBDs of $\mathbb{C}P^2\#4\overline{\mathbb{C}P^2}$

The operations relating each diagram in Fig. 17 are described below:

(A_1) Blowup the corner of the ATBD (A_5) of Fig. 16;
(A_2) Applied one nodal trade, getting a (0, 1)-node;
(A_3) Mutated (0, 1)-node.
(A_4) Mutated both (1, −1)-nodes.

3.3 ATFs of $\mathbb{C}P^2\#5\overline{\mathbb{C}P^2}$

The operations relating the (A)'s diagrams in Fig. 18:

(A_1) Blowup the corner of the ATBD (A_3) of Fig. 17;
(A_2) Applied one nodal trade, getting a (0, 1)-node;
(A_3) Mutated (0, 1)-node.

Following the top arrow towards the (B)'s diagrams in Fig. 18 we:

(B_1) Mutated both (0, 1)-nodes and applied one nodal trade, getting a (1, 1)-node;
(B_2) Mutated all three (−1, −1)-nodes.

To obtain (C_1) ATDB we:

(C_1) Mutated both (1, 0)-nodes.

The ATDB of Fig. 2 is a $\pi/2$ rotation of the ATBD (B_2) in Fig. 18. The ATBD (C_1) in Fig. 18 is used to perform another blowup. Note that the mutation form (A_3) to (C_1) is described in Sect. 2.2 (see Fig. 10). In Fig. 18, we change the grid from the (A_1) to the (C_1) ATBD so that all the edges have integer affine length with respect to the new grid.

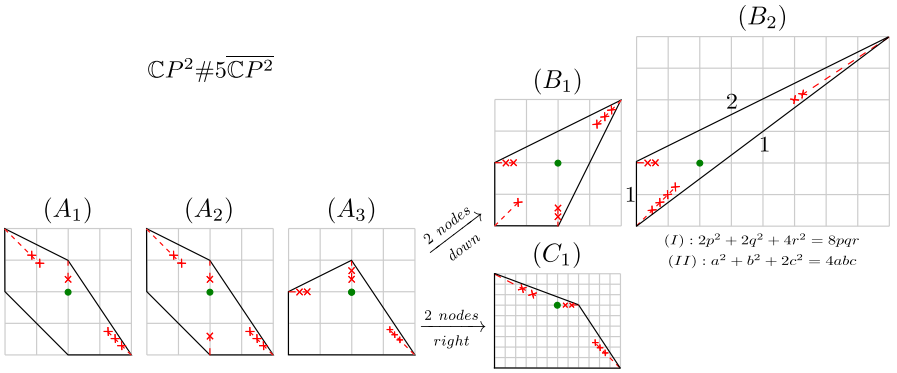

Fig. 18 ATBDs of $\mathbb{C}P^2\#5\overline{\mathbb{C}P^2}$

3.4 ATFs of $\mathbb{C}P^2\#6\overline{\mathbb{C}P^2}$

In Fig. 19 we show how to get both ATBDs of Fig. 2.

The operations relating the (A)'s diagrams in Fig. 19 are described below:

(A_1) Blowup the corner of the ATBD (C_1) of Fig. 18;
(A_2) Applied one nodal trade, getting a $(1, 0)$-node;
(A_3) Mutated both $(-1, 0)$-nodes.

Following the top arrow towards the (B)'s diagrams in Fig. 19 we:

(B_1) Mutated the $(0, 1)$-node;
(B_2) Mutated all three $(0, -1)$-nodes.

Following the bottom arrow from the (A_3) ATBD towards the (C_1) ATBD in Fig. 19, we:

(C_1) Mutated only one $(0, -1)$-node;
(C_2) Mutated all three $(-1, 1)$-nodes.

Note that from (A_3) we could have mutated to an ATBD equivalent to (B_2) directly, by mutating both $(0, -1)$-nodes. Note that (B_2) is related to minimal solutions of the Markov type equations. We mutated to (B_1) because we will use it to perform almost toric blowup in the next section. We will also perform an almost toric blowup in the ATBD (C_2).

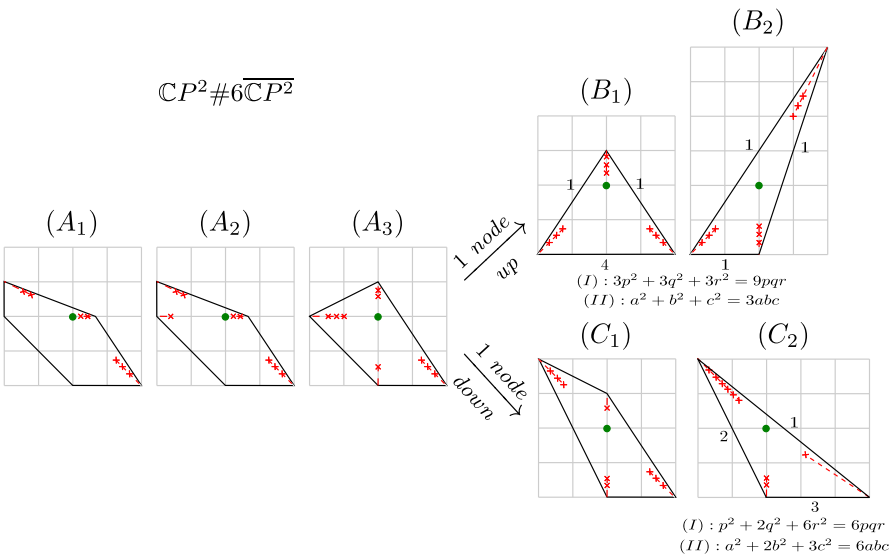

Fig. 19 ATBDs of $\mathbb{C}P^2\#6\overline{\mathbb{C}P^2}$

3.5 ATFs of $\mathbb{C}P^2\#7\overline{\mathbb{C}P^2}$

In the remaining sections, *when performing almost toric blowups* (Sect. 2.4) we refer to the length of an almost toric blowup in a given ATBD according to the grid depicted. When getting to ATBDs of triangular shape, the depicted affine lengths are scaled as before to form a Markov type II triple (Definition 2.6) for the equation length related to the corresponding ATBD (Definition 2.13). Recall that the invariant direction of the monodromy is parallel to the edge containing the point we blowup.

To get the ATBDs (A_1) and (D_1) in Fig. 20, we apply an almost toric blowup of length 4 to the ATBDs (B_1) and (C_2) of Fig. 19. So the area of the exceptional divisor is 4. Since 4 is also the distance from the monotone fibre to the bottom edge, which the area of an Maslov 2 disk lying over the vertical segment, we remain monotone.

After several mutations, we are able to get the ATBDs of Fig. 3. As usual, we get ATBDs (B_3) and (C_2) to have space for the next blowups. In Fig. 21, we change the grid of the ATBD (C_3) so that all the edges have integer affine length with respect to the new grid.

The operations relating the (A)'s diagrams in Fig. 20 are described below:

- (A_1) Applied an almost toric blowup of length 4 in the edge of the ATBD (B_1) of Fig. 19;
- (A_2) Transferred the cut towards the right edge, getting a $(-1, 0)$-node. (See beginning of Sect. 2.4).

Following the top arrow towards the (B)'s diagrams in Fig. 20 we:

- (B_1) Mutated only one $(0, -1)$-node;
- (B_2) Mutated the $(-1, -1)$-node;
- (B_3) Mutated all four $(0, 1)$-nodes.

Following the bottom arrow from the (A_2) ATBD towards the (C)'s diagrams in Fig. 20 we:

- (C_1) Mutated all three $(0, -1)$-nodes;
- (C_2) Mutated all six $(0, 1)$-nodes.

Now we describe the operations relating the (D)'s diagrams in Fig. 20:

- (D_1) Applied an almost toric blowup of length 2 in the edge of the ATBD (C_2) of Fig. 19;
- (D_2) Transferred the cut towards the left edge, getting a $(1, 0)$-node;
- (D_3) Mutated all six $(1, -1)$-nodes.

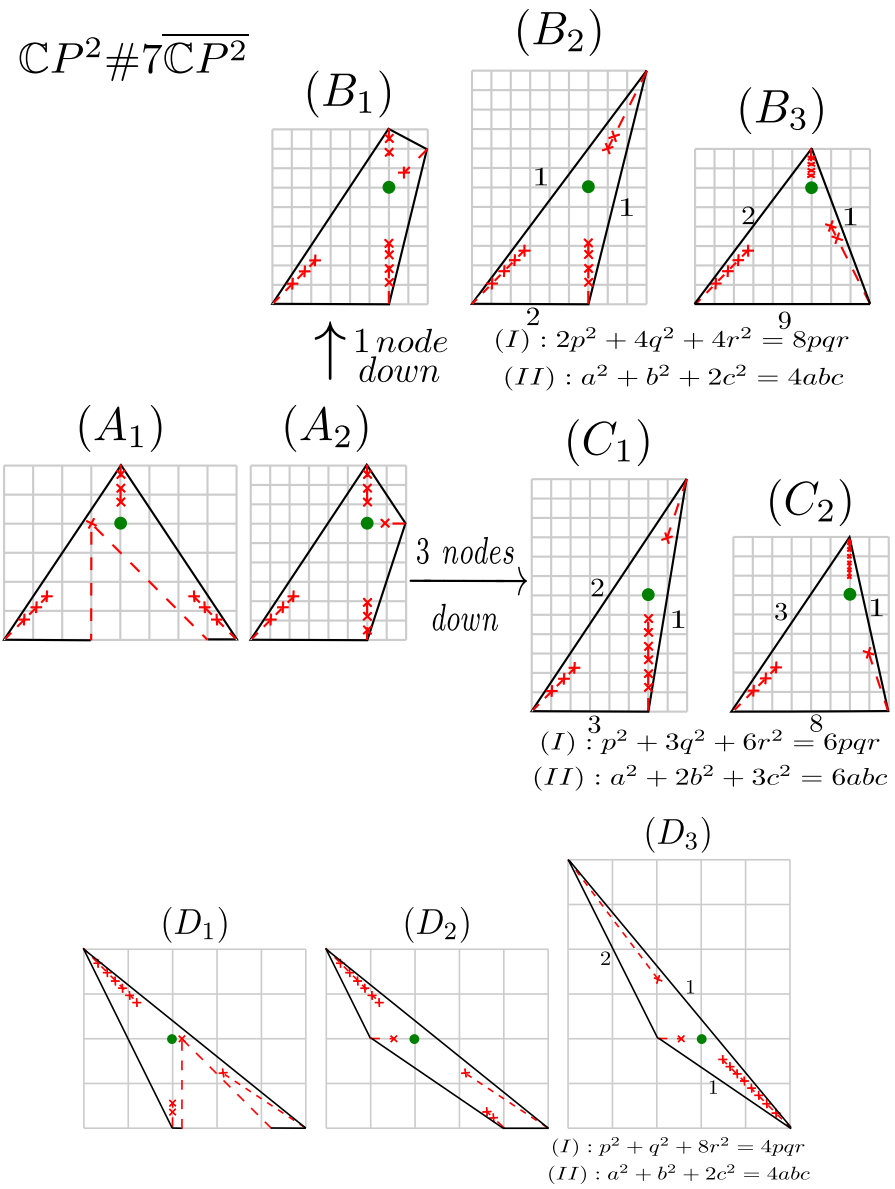

Fig. 20 ATBDs of $\mathbb{C}P^2\#7\overline{\mathbb{C}P^2}$

3.6 ATFs of $\mathbb{C}P^2\#8\overline{\mathbb{C}P^2}$

We again blowup on edges of different ATBDs of $\mathbb{C}P^2\#7\overline{\mathbb{C}P^2}$, namely (B_3) and (C_2) in Fig. 20. After mutations we get the ATBDs of Fig. 4.

The operations relating the (A)'s diagrams in Fig. 21 are described below:

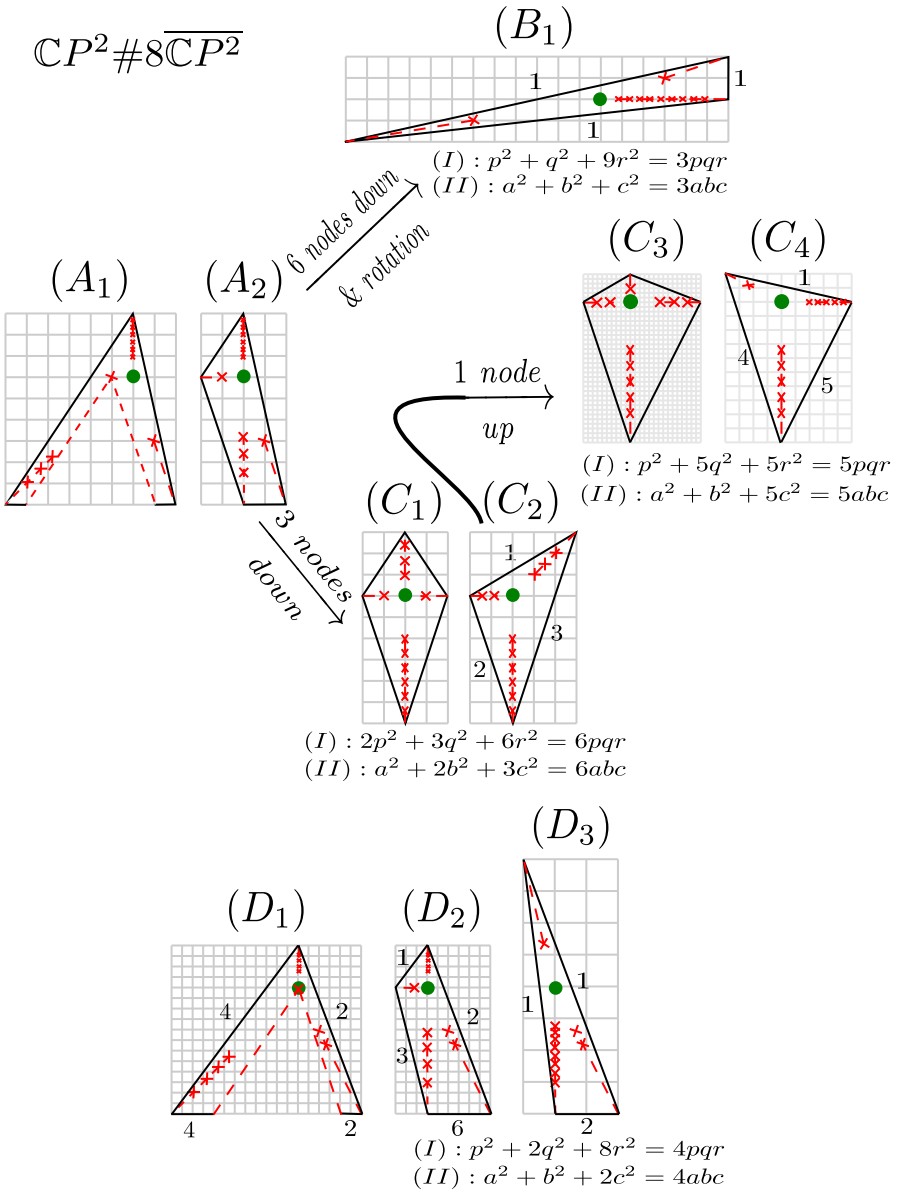

Fig. 21 ATBDs of $\mathbb{C}P^2\#8\overline{\mathbb{C}P^2}$

(A_1) Applied an almost toric blowup of length 6 in the edge of the ATBD (C_2) of Fig. 20;

(A_2) Transferred the cut towards the left edge, getting a $(1, 0)$-node. (See beginning of Sect. 2.4).

Following the top arrow towards the (B)'s diagrams in Fig. 21 we:

(B_1) Mutated all six $(0,-1)$-nodes and applied the counter-clockwise $\pi/2$ rotation $(\in SL(2,\mathbb{Z}))$.

Following the bottom arrow from the (A_2) ATBD towards the (C)'s diagrams in Fig. 21:

(C_1) Mutated only three $(0,-1)$-nodes;
(C_2) Mutated the $(-1,0)$-node;
(C_3) Mutated only one $(0,1)$-node;
(C_4) Mutated both $(1,0)$-nodes.

Finally, we describe the operations relating the (D)'s diagrams in Fig. 21:

(D_1) Applied an almost toric blowup of length 6 in the edge of the ATBD (B_3) of Fig. 20 (the grid was refined so the blowup has length 12 on the new grid);
(D_2) Transferred the cut towards the left edge, getting a $(1,0)$-node;
(D_3) Mutated all four $(0,-1)$-nodes.

3.7 ATFs of $\mathbb{C}P^1 \times \mathbb{C}P^1$

We finish by describing the ATBD of triangular shape for $\mathbb{C}P^1 \times \mathbb{C}P^1$ appearring in Fig. 1. Apply the counter-clockwise $\pi/2$ rotation $(\in SL(2,\mathbb{Z}))$ to the ATBD (A_3) of Fig. 22 and get the ATBD in Fig. 1.

The operations relating the diagrams in Fig. 22 are described below:

(A_1) Standard moment polytope of $\mathbb{C}P^1 \times \mathbb{C}P^1$;
(A_2) Applied two nodal trades, getting a $(-1,1)$ and $(1,-1)$ nodes;
(A_3) Mutated the $(-1,1)$-node.

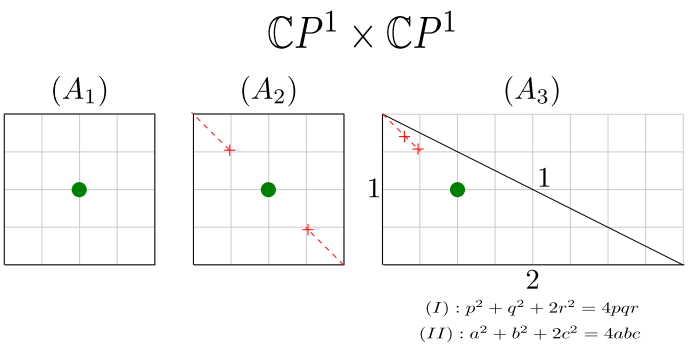

Fig. 22 ATBDs of $\mathbb{C}P^1 \times \mathbb{C}P^1$

4 Mutations and ATBDs of triangular shape

Let Δ be an ATBD of length type (k_1a^2, k_2b^2, k_3c^2), where (a, b, c) are Markov triples for Eq. (2.2). Assume that Δ has a monotone fibre (not lying over a cut). Let $\mathbf{u}_1, \mathbf{u}_2, \mathbf{u}_3$ be primitive vectors in the direction of the edges of Δ, so that $k_1a^2\mathbf{u}_1 + k_2b^2\mathbf{u}_2 + k_3c^2\mathbf{u}_3 = 0$. Up to $SL(2, \mathbb{Z})$, we can assume that $\mathbf{u}_3 = (1, 0)$. Let $\mathbf{w}_i$ be the direction of the cut pointing towards the edge whose direction is $\mathbf{u}_i$, see Fig. 23. Let n_i be the number of nodes in the cut $\mathbf{w}_i$. Write $\mathbf{w}_1 = (x, p)$ and $\mathbf{w}_2 = (y, q)$.

The monodromy around a clockwise oriented loop surrounding n nodes with eigendirection given by the primitive vector (s, t) is given by [31, (4.11)]:

$$\begin{bmatrix} 1 - st & s^2 \\ -t^2 & 1 + st \end{bmatrix}^n = \begin{bmatrix} 1 - nst & ns^2 \\ -nt^2 & 1 + nst \end{bmatrix} \tag{4.1}$$

So we have $\mathbf{u}_1 = (1 - n_2yq, -n_2q^2)$ and $\mathbf{u}_2 = (1 + n_1xp, n_1p^2)$. Note that $n_1p^2 = |\mathbf{u}_3 \wedge \mathbf{u}_2|$ and $n_2q^2 = |\mathbf{u}_1 \wedge \mathbf{u}_3|$, which is invariant under $SL(2, \mathbb{Z})$ (where $|\mathbf{u} \wedge \mathbf{w}|$ is the determinant of the matrix formed by the column vectors $\mathbf{v}$, $\mathbf{w}$). So, $|\mathbf{u}_2 \wedge \mathbf{u}_1| = n_3r^2$ for some $r \in \mathbb{Z}$.

Proposition 4.1 *We have that:*

$$\frac{n_1p^2}{k_1a^2} = \frac{n_2q^2}{k_2b^2} = \frac{n_3r^2}{k_3c^2} \tag{4.2}$$

We denote the above value by λ.

Proof Follows immediately from $k_1a^2\mathbf{u}_1 + k_2b^2\mathbf{u}_2 + k_3c^2\mathbf{u}_3 = 0$, that $\frac{n_1p^2}{k_1a^2} = \frac{n_2q^2}{k_2b^2}$. Apply a $SL(2, \mathbb{Z})$ map to conclude that it is also equal to $\frac{n_3r^2}{k_3c^2}$. □

It also follows from from $k_1a^2\mathbf{u}_1 + k_2b^2\mathbf{u}_2 + k_3c^2\mathbf{u}_3 = 0$ and the Markov type II equation that:

$$Kk_1k_2k_3abc = k_1a^2 + k_2b^2 + k_3c^2 = n_2yqk_1a^2 - n_1xpk_2b^2 \tag{4.3}$$

Fig. 23 ATBD Δ

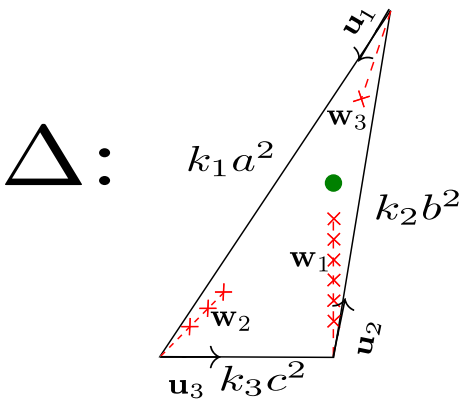

It is worth noting that

$$k_1 a a' = k_2 b^2 + k_3 c^2 \tag{4.4}$$

Lemma 4.2 *If we mutate all the $\boldsymbol{w}_1$-nodes of Δ we obtain an ATBD of length type $(k_1 a'^2, k_2 b^2, k_3 c^2)$, where $a' = K k_2 k_3 bc - a$, i.e., (a', b, c) is the mutation of (a, b, c) with respect to a. Similarly, if we mutate all $\boldsymbol{w}_2$-nodes, respectively $\boldsymbol{w}_3$-nodes, of Δ, the length type changes according to the mutation of (a, b, c) with respect to b, respectively, c.*

Proof We need to prove that the affine lengths of the edges of the mutated ATBD are proportional to $(k_1 a'^2, k_2 b^2, k_3 c^2)$. For convenience we rescale the lengths of the edges of Δ by a'.

The mutation aligns the edges in directions $\mathbf{u}_2$, $\mathbf{u}_3$, to get an edge of affine length $a'(k_3 c^2 + k_2 b^2) = a k_1 a'^2$. As in Fig. 6, assume we kept $\mathbf{w}_2$ fixed and mutated $\mathbf{w}_3$. The mutation divides the edge in direction $\mathbf{u}_1$ into two edges with affine lengths α and $a' k_1 a^2 - \alpha$. Say that the edge of length $a' k_1 a^2 - \alpha$ is opposite the w_2-eigenray. It is enough to show that $\alpha = a k_3 c^2$, so $a' k_1 a^2 - \alpha = a(a a' k_1 - k_3 c^2) = a k_2 b^2$.

We have that for some $\beta < 0$:

$$a' k_3 c^2 \mathbf{u}_3 = \beta \mathbf{w}_1 - \alpha \mathbf{u}_1 \tag{4.5}$$

Hence

$$0 = \beta p + \alpha n_2 q^2 \tag{4.6}$$

$$a' k_3 c^2 = \beta x + \alpha(n_2 y q - 1) \tag{4.7}$$

By Eqs. (4.2) and (4.6), we have:

$$\beta = -\alpha \frac{n_2 q^2}{p} = -\alpha \frac{k_2 b^2 n_1 p}{k_1 a^2} \tag{4.8}$$

Plugging into Eq. (4.7) and using Eq. (4.3), we get:

$$\begin{aligned} a' k_3 c^2 &= \frac{\alpha}{a}\left[\frac{1}{k_1 a}\left(-k_2 b^2 n_1 p x + k_1 a^2 n_2 y q\right) - a\right] \\ &= \frac{\alpha}{a}\left[K k_2 k_3 bc - a\right] = a' \frac{\alpha}{a} \end{aligned} \tag{4.9}$$

So indeed $\alpha = a k_3 c^2$. □

A direct consequence of Proposition 4.1 and that Δ is length-related to the Markov type II equation (2.2) is

Corollary 4.3 *Consider the ATBD Δ. The numbers $n_1 p^2 = |\boldsymbol{u}_3 \wedge \boldsymbol{u}_2|$, $n_2 q^2 = |\boldsymbol{u}_1 \wedge \boldsymbol{u}_3|$, $n_3 r^2 = |\boldsymbol{u}_2 \wedge \boldsymbol{u}_1|$ are so that (p, q, r) is a Markov type I triple for the equation:*

$$n_1 p^2 + n_2 q^2 + n_3 r^2 = \sqrt{d n_1 n_2 n_3}\, pqr, \quad (2.1)$$

where $d = \frac{K^2 k_1 k_2 k_3}{\lambda}$.

It follows then from the Lemma 4.2 and Proposition 4.1:

Corollary 4.4 *If we mutate all the* $\boldsymbol{w}_1$*-nodes of* Δ *we obtain an ATBD of node type* $((n_1, p'), (n_2, q), (n_3, r))$*, where* (p', q, r) *is a mutation of the* (p, q, r) *Markov type I triple. Analogously, for the other* $\boldsymbol{w}_i$*-nodes.*

We can verify for each ATBD in Figs. 1, 2, 3 and 4, that the value of d in Corollary 4.3 is equal to the degree of the corresponding del Pezzo. Note that λ, K, k_1, k_2 and k_3 are invariant under *total mutation* in a ATBD of triangular shape. For instance, let's check $d = 1$ for the bottom right diagram on Fig. 4—(C_4) in Fig. 21. We already know the length of the edges: $k_1 a^2 = 1$, $k_2 b^2 = 5$, $k_3 c^2 = 4$. So $k_1 = a = b = 1$ and $k_2 = 5$. To also satisfy a Markov type II equation (2.2):

$$10 = k_1 a^2 + k_2 b^2 + k_3 c^2 = K k_1 k_2 k_3 abc = 5 K k_3 c;$$

we must have $c = 2$ and $k_3 = K = 1$. The primitive vectors $\mathbf{u}_1, \mathbf{u}_2, \mathbf{u}_3$ are $(-9, 2)$, $(1, -3)$, $(1, 2)$. Their pairwise determinants are 25, 5 and 20, which, when accordingly divided by the affine lengths 5, 1 and 4, gives $\lambda = 5$ (see Proposition 4.1). Hence, $d = K^2 k_1 k_2 k_3 / \lambda = 1$. The computations for the Markov type I and II equations related to the other ATBDs of Figs. 1, 2, 3 and 4 work in a similar fashion.

Instead of checking all the equations one-by-one, we can show that any ATBD of node type $((n_1, p), (n_2, q), (n_3, r))$ is node-related to the corresponding Markov type I equation:

Theorem 4.5 *Let* Δ' *be an ATBD of node type* $((n_1, p), (n_2, q), (n_3, r))$*, such that the total space* $X_{\Delta'}$ *of the corresponding ATF is monotone. Then* (p, q, r) *is a Markov type I triple for* (2.1)*.*

Proof We will look at the self-intersection of the anti-canonical divisor class inside the limit orbifold X_o, as defined in [4, Definition B]. Name (n_1, p)-vertex, respectively (n_2, q)-vertex, (n_3, r)-vertex, the image of the orbifold point that is associated with the pair (n_1, p), respectively (n_2, q), (n_3, r). The second homology of the limit orbifold X_o is one-dimensional, since the moment polytope is a triangle, so topologically X_o is a rational homology four-ball attached to a two-sphere. Indeed, the complement of $\mathcal{A}$, defined as the (pre-image of the) edge not containing the (n_1, p)-vertex, is an orbifold ball whose boundary is a visible lens space of the form $L(n_1 p^2, n_1 px - 1)$, see [31, Section 9.1, Definition 9.8, Proposition 9.9]. So, the Mayer–Vietoris exact sequence gives us:

$$0 \to H_2(\mathcal{A}; \mathbb{Z}) = \mathbb{Z} \to H_2(X_o; \mathbb{Z}) \to H_1(L(n_1 p^2, n_1 px - 1); \mathbb{Z}) = {}^{\mathbb{Z}}\!/_{n_1 p^2} \to 0. \tag{4.10}$$

Denote by H the generator of $H_2(X_o; \mathbb{Z})$. By the exact sequence (4.10), we have that $[\mathcal{A}] = n_1 p^2 H \in H_2(X_o; \mathbb{Z})$. If we name $\mathcal{B}$, respectively $\mathcal{C}$, the (pre-image of the) edge not containing the (n_2, q)-vertex, respectively (n_3, r)-vertex, we have that $[\mathcal{B}] = n_2 q^2 H \in H_2(X_o; \mathbb{Z})$ and $[\mathcal{C}] = n_3 r^2 H \in H_2(X_o; \mathbb{Z})$.

Claim 4.6 X_o is monotone, with same monotonicity constant as $X_{\Delta'}$. (Same definition as in Sect. 2.3 [Eq. (2.3)]—see [6, Proposition 4.3.4, Examples 4.3.6a, 4.3.6b] for definition of Chern class in orbifolds.) In particular, $c_1^2(X_o) = d$. Moreover the cycle $[\mathcal{A}] + [\mathcal{B}] + [\mathcal{C}]$ is Poincaré dual to the first Chern class.

Proof Consider a fibre T and disks living over paths connecting T to the edges in the moment polytope of the limit orbifold X_o. These disks generate $H_2(X_o, T; \mathbb{Q})$, so some integer linear combination is a multiple of H viewed in $H_2(X_o, T, \mathbb{Z})$. Therefore we can complete these disks with a 2-chain in T, to get a cycle $m\hat{H}$ representing a multiple of H lying away from the orbifold points.

The complement of small neighbourhoods around the orbifold points can be symplectically embedded into $X_{\Delta'}$, up to sliding the nodes close enough to the edges, see [37, Figure 7, Section 4.2]. We assume it contains $m\hat{H}$ and see $m\hat{H} \subset X_{\Delta'}$. Hence the Chern class and symplectic area of $[m\hat{H}]$ coincide in both $X_{\Delta'}$ and X_o. So, we get monotonicity for X_o with same monotonicity constant. In particular, $c_1^2(X_o) = d$. Now, the cycle living over the edge is Poincaré dual to $c_1(X_{\Delta'})$ [31, Proposition 8.2]. Its intersection with $m\hat{H}$ in $X_{\Delta'}$ is the same as the intersection of $m\hat{H}$ with $\mathcal{A}+\mathcal{B}+\mathcal{C}$ in X_o. Since $H_2(X_o; \mathbb{Z}) = \mathbb{Z}$ and the Chern classes of $[m\hat{H}]$ coincide in both $X_{\Delta'}$ and X_o, we conclude that $[\mathcal{A}] + [\mathcal{B}] + [\mathcal{C}]$ is Poincaré dual to $c_1(X_o)$. □

Claim 4.7 The self-intersection of H is

$$H \cdot H = \frac{1}{n_1 n_2 n_3 p^2 q^2 r^2}. \tag{4.11}$$

Proof The degree of the orbifold point common to $\mathcal{A}$ and $\mathcal{B}$ is the determinant of the primitive vectors of the edges, i .e ., $n_3 r^2$. Hence, $[\mathcal{A}]\cdot[\mathcal{B}] = n_1 p^2 H \cdot n_2 q^2 H = 1/n_3 r^2$ ([4, Theorem 3.2]), and the claim follows. □

It follows from Claims 4.6 and 4.7 that:

$$\begin{aligned} &([\mathcal{A}] + [\mathcal{B}] + [\mathcal{C}]) \cdot ([\mathcal{A}] + [\mathcal{B}] + [\mathcal{C}]) \\ &= (n_1 p^2 + n_2 q^2 + n_3 r^2) H \cdot (n_1 p^2 + n_2 q^2 + n_3 r^2) H \\ &= \frac{(n_1 p^2 + n_2 q^2 + n_3 r^2)^2}{n_1 n_2 n_3 p^2 q^2 r^2} = d. \end{aligned} \tag{4.12}$$

Taking the square root, we get the Markov type I equation (2.1). □

Proposition 4.8 (Section 3.5 of [20]) *All Markov type I equations* (2.1) *with* $n_1 + n_2 + n_3 + d = 12$, *and* $n_1, n_2, n_3, d \in \mathbb{Z}_{>0}$ *are the ones appearing in Figs.* 1, 2, 3 *and* 4.

And from the proposition below and Corollary 4.4, it follows that each ATBD of Figs. 1, 2, 3 and 4, gives rise to infinitely many ones.

Proposition 4.9 (Section 3.7 of [20]) *Any solution of the Markov type I equations appearing in Figs.* 1, 2, 3, 4, *can be reduced to a minimal solution via a series of mutations. Moreover, two out of the three possible mutations increase the sum* $p+q+r$ *and the other reduces it.*

From Theorem 4.5 and the work of Karpov–Nogin [20] we see that:

Proposition 4.10 *Our list described in Figs. 1, 2, 3 and 4, together with its total mutations, describes all ATBDs of triangular shape.*

Proof Indeed, given an ATBD of triangular shape, its Euler characteristic is given by $n_1+n_2+n_3$ [31, Section 8.1], and the total space is $\mathbb{C}P^2\#k\overline{\mathbb{C}P^2}$ for $k = n_1+n_2+n_3-3$, or $\mathbb{C}P^1 \times \mathbb{C}P^1$ if $n_1+n_2+n_3 = 4$ [23, Table 1]. Hence, its second homology has rank $n_1+n_2+n_3-2$. But an ATBD of triangular shape has $(n_1-1)+(n_2-1)+(n_3-1)$ Chern zero Lagrangian spheres in linearly independent homology classes. They are visible surfaces ([31, Definition 7.2]) living over the segment inside the cut between two nodes. (In fact, each n_i set of nodes in the same cut gives us $\binom{n_i}{2}$ Lagrangian spheres living in n_i-1 linearly independent homology classes. We check linear independence of these classes by looking at intersections between such spheres.) Therefore, the total space must be monotone, hence a del Pezzo surface of degree d, $1 \leq d \leq 9$. The result follows from Theorem 4.5, Propositions 4.8, 4.9 and Corollary 4.4. □

5 Infinitely many tori

We name $\Theta^{n_1,n_2,n_3}_{p,q,r}$ the monotone fibre of a monotone ATBD of node-type $((n_1, p), (n_2, q), (n_3, r))$ (see Propositions 4.9, 4.10). In this section we show that these tori live in mutually different symplectomorphism classes, completing the proof of Theorem 1.1(a). We also show that there are infinitely many symplectomorphism classes formed by the monotone tori $T_1(a, b)$ in $\mathbb{C}P^2\#\overline{\mathbb{C}P^2}$, depicted in Fig. 7, proving 1.1(b). To finish the section we prove Theorem 1.6.

We recall the definition of the boundary Maslov-2 convex hull:

Definition 5.1 ([37] (Definition 4.2)) Let L be a Lagrangian submanifold of a symplectic manifold (M, ω), endowed with a regular almost complex structure J. The *boundary Maslov-2 convex hull* of L, $\mho_L$, is the convex hull in $H_1(L; \mathbb{R})$ generated by the subset $\{\partial\beta \in H_1(L; \mathbb{Z}) \mid \beta \in \pi_2(M, L) \subset H_2(M, L)$, such that the algebraic count of Maslov index 2 J-holomorphic discs in the class β is non-zero$\}$.

5.1 ATBDs of triangular shape

The Theorem 1.1(a) follows from Theorem 5.2 and the invariance of the boundary Maslov two convex hull for monotone Lagrangian [37, Corollary 4.3].

Theorem 5.2 *The boundary Maslov two convex hull of $\Theta^{n_1,n_2,n_3}_{p,q,r}$ is dual to the moment polytope of the corresponding limit orbifold. More specifically, if $\boldsymbol{u}_1$, $\boldsymbol{u}_2$ and $\boldsymbol{u}_3$ are the primitive vectors related to the edges of the moment polytope of limit orbifold (oriented as in Fig. 23), then the boundary convex hull $\mho_{\Theta^{n_1,n_2,n_3}_{p,q,r}}$ is a triangle with vertices in $\bar{\boldsymbol{u}}_1$, $\bar{\boldsymbol{u}}_2$, $\bar{\boldsymbol{u}}_3$, up to $SL(2, \mathbb{Z})$ – where $\overline{(x, y)} = (-y, x)$. Moreover, the affine lengths of the edges of $\mho_{\Theta^{n_1,n_2,n_3}_{p,q,r}}$ are n_1p, n_2q, n_3r.*

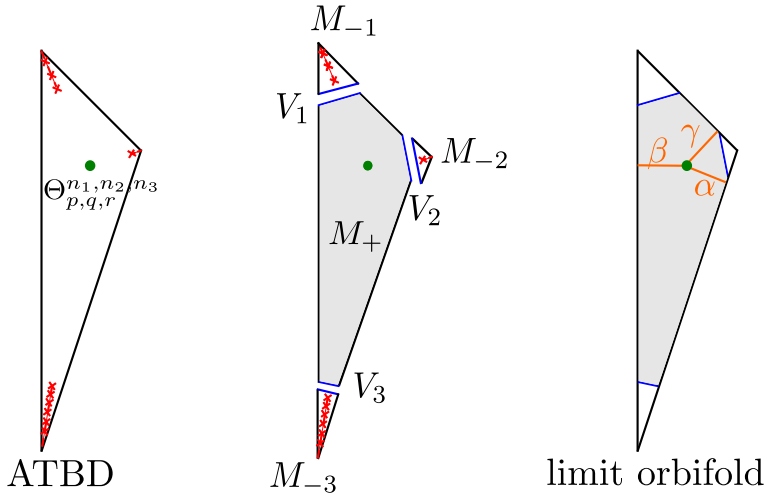

Fig. 24 We embed $M_+ \subset M$ into the limit orbifold and pullback J-holomorphic disks from the limit orbifold. The boundary of these disks correspond to the vertices of $\mho_{\Theta^{n_1,n_2,n_3}_{p,q,r}}$

Proof The proof of the first part is totally analogous to the proof of Theorem 1.1 [37, Section 4], so we will only sketch it here. Denote by M the del Pezzo surface described by an ATBD of triangular shape Δ, by $\overline{M^{\infty}_{+}}$ the limit orbifold, and by $\mathcal{A}$, $\mathcal{B}$, $\mathcal{C}$ the pre-image of the edges of the moment polytope of $\overline{M^{\infty}_{+}}$, see Fig. 24.

The setup for the proof is as follows. We first consider the symplectic submanifolds M_{-i}'s formed by the pre-image of an open sector of the ATBD that encloses the n_i nodes, $i = 1, 2, 3$, contained in the same cut (as in Fig. 24). The boundary of the M_{-i}'s are contact hypersurfaces V_i's of M and are visible lens spaces [31, Definition 9.8, Proposition 9.9]. We embed $M_+ = M \setminus (M_{-1} \cup M_{-2} \cup M_{-3})$ inside the limit orbifold; we pullback the standard complex structure from the limit orbifold to M_+ and extend it to M (see the similar setup in [37, Section 4.2]). Call J this almost complex structure. We also pullback the Maslov index 2 holomorphic disks α, β, γ [5, Corollary 6.4], which live in the complement of the orbifold points in the limit orbifold—we abuse notation and also call by α, β, γ their pullback to M. The boundary of these disks corresponds to the collapsing cycle associated to the respective edge (the cycle in T^2 corresponding to the stabiliser of a point living over an edge), and therefore can be identified with the vectors $\bar{\mathbf{u}}_i$, $i = 1, 2, 3$ as in the statement of the Theorem 5.2 [5, Corollary 6.4].

The core idea of the proof is that any Maslov index 2 J-holomorphic disk with boundary in $\Theta^{n_1,n_2,n_3}_{p,q,r}$ gives rise to a degenerated holomorphic disk in the limit orbifold upon stretching the neck [3, Section 3.4], [8, Section 1.3] with respect to the contact hypersurface hypersurface $V = V_1 \cup V_2 \cup V_3$. Looking at the intersection of degenerated disk with $\mathcal{A}$, $\mathcal{B}$, $\mathcal{C}$, implies that *the boundary of the disks* α, β, γ *will correspond to the vertices of* $\mho_{\Theta^{n_1,n_2,n_3}_{p,q,r}}$ as described in the statement of Theorem 5.2. To prove that, we consider a Maslov index 2 J-holomorphic disk u with boundary on $\Theta^{n_1,n_2,n_3}_{p,q,r}$. We only need to prove the following Lemma similar to [37, Lemma 4.9]:

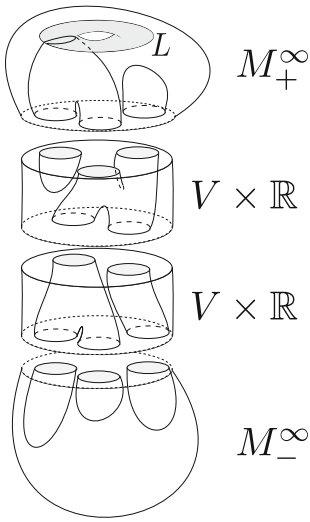

Fig. 25 [37, Figure 6] Example of neck-stretching limit of a J-holomorphic disk. In our scenario, $L = \Theta^{n_1,n_2,n_3}_{p,q,r}$ and $V = V_1 \cup V_2 \cup V_3$ is disconnected

Lemma 5.3 *Assume that the algebraic count of J-holomorphic disks in $[u] \in \pi_2(M, \Theta^{n_1,n_2,n_3}_{p,q,r})$ is non-zero. Then the class $\partial[u] \in H_1(\Theta^{n_1,n_2,n_3}_{p,q,r}; \mathbb{Z})$ lies in the convex hull generated by $\partial[\alpha]$, $\partial[\beta]$, $\partial[\gamma]$.*

Sketch of proof We stretch the neck with respect to the contact disconnected hypersurface $V = V_1 \cup V_2 \cup V_3$, [3, Section 3.4], [8, Section 1.3] (see also [37, Section 3]), obtaining a limit $M^\infty = M_+^\infty \cup M_-^\infty$, where M_+^∞ is the symplectic completion of M_+ while M_-^∞ is the symplectic completion of $M_- = M_{-1} \cup M_{-2} \cup M_{-3}$, with the symplectic form scaled by $e^{-\infty} = 0$, see [37, Section 3.1] for details. Our focus is in M_+^∞, where the symplectic form matches the standard one from the symplectic completion of M_+. Neck-stretching can be thought as a limit $M^n \to M^\infty$, as $n \to \infty$, of inserting necks of finite length [37, Section 3.1], where M^n is symplectomorphic to M. As in the proof of [37, Lemma 4.9], we see that the map u gives rise to J^n-holomorphic maps $u^n : \mathbb{D} \to M^n$, for the almost complex structure J^n corresponding to M^n as in [37, Section 3.2].

By the compactness Theorems [3, Theorem 10.6], [8, Theorem 1.6.3] (also reproduced in [37, Theorem 3.3]), there exists a subsequence that converges to a stable curve of height k, for some $k \geq 1$ (see Fig. 25).

Lemma 5.4 *The top part of the neck-stretching splitting M_+^∞ (endowed with its symplectic form ω_+^∞ and almost complex structure J_+^∞, as described in* [37, Sections 3.1, 3.2]*) is symplectomorphic to the complement of the orbifold points in the limit orbifold (endowed with the standard toric complex structure and symplectic form).*

Proof It follows from our choice of almost complex structure J and [37, Corollary 3.2], as in [37, Lemma 4.7] □

The part of the J-holomorphic building (stable curve of some height) lying in M_+^∞ (see Fig. 25), compactifies to a degenerated J-holomorphic disk u_+^∞ in the limit

orbifold $\overline{M_+^\infty}$, (see [4, Definition A] for the definition of J-holomorphic curves in orbifolds) having the same boundary as u upon the natural identification of $\Theta_{p,q,r}^{n_1,n_2,n_3}$ with a fibre in the limit orbifold. This is a consequence of [37, Corollary 3.2]. The domain of the degenerated J-holomorphic disk u_+^∞ will be a disk union a (possibly zero) finite number of spheres. Positivity of intersection in the limit orbifold [4, Theorem 3.2] implies that u_+^∞ intersects the divisors $\mathcal{A}$, $\mathcal{B}$ and $\mathcal{C}$ positively (note that if any of the divisors had negative self-intersection, we would not be able to draw such a conclusion, since a multiple of this divisor could be a part of the degenerated disk u_+^∞). This allow us to conclude that the class of the boundary of u_+^∞, and hence the class of the boundary of u, lies in the convex hull generated by $\partial\alpha$, $\partial\beta$, $\partial\gamma$. (Note that the plane of Maslov index 2 classes in the limit orbifold projects injectively to $H_1(\Theta_{p,q,r}^{n_1,n_2,n_3};\mathbb{Z})$ under the boundary map.) We conclude the proof of Lemma 5.10 and therefore the first part of the Theorem 5.2. □

For the second part, we use the notation in the description of Δ in Sect. 4, see Fig. 23. The primitive vectors dual to the moment polytope of the limit orbifold are $\bar{\mathbf{u}}_3 = (0,1)$, $\bar{\mathbf{u}}_1 = (n_2q^2, 1-n_2yq)$, $\bar{\mathbf{u}}_2 = (-n_1p^2, 1+n_1xp)$, which are respectively orthogonal to $\mathbf{u}_3$, $\mathbf{u}_1$, $\mathbf{u}_2$. Hence the affine length of the edges $\bar{\mathbf{u}}_1 - \bar{\mathbf{u}}_3 = n_2q(q,-y)$ and $\bar{\mathbf{u}}_2 - \bar{\mathbf{u}}_3 = n_2p(-p,x)$ of $\mathcal{O}_{\Theta_{p,q,r}^{n_1,n_2,n_3}}$ are respectively n_2q and n_1p. After applying a $SL(2,\mathbb{Z})$ map, we can do the same analysis to conclude that the affine length of the edge $\bar{\mathbf{u}}_1 - \bar{\mathbf{u}}_2$ is n_3r. □

5.2 On $\mathbb{C}P^2\#\overline{\mathbb{C}P^2}$

This section is devoted to proving Theorem 1.1(b). We start with ATBDs of $\mathbb{C}P^2$ with two nodes and one corner (rank zero elliptic singularity) of length-type $(a^2, b^2, 1)$, where $a^2 + b^2 + 1 = 3ab$, as depicted in Fig. 7. We assume $a < b$, and scale the symplectic form so that the affine length of the edges are $3, 3a^2, 3b^2$. We need to blow up so that the area of the exceptional divisor $\mathcal{E}$ is 1/3 of the area of the line in $\mathbb{C}P^2$, since $c_1(\mathcal{E}) = 1$ and $c_1(\text{line}) = 3$. The area of the anti-canonical divisor $3[\mathbb{C}P^1]$, represented by the pre-image of the edges of the ATBD [31], is $3a^2 + 3b^2 + 3 = 9ab$. Hence, we choose the blowup size for which the symplectic area $\omega \cdot \mathcal{E}$ is equal to ab (see Fig. 7). We note that we have space to blowup, since $3a^2 - ab = ab' > 0$ and $3b^2 - ab = ba' > 0$. We name M the blowup $\mathbb{C}P^2\#\overline{\mathbb{C}P^2}$ and $T_1(a,b)$ the monotone torus.

We proceed as in the proof of Theorem 5.2, where we apply neck-stretching, with respect to the union of contact lens spaces $V = V_1 \cup V_2$, where each V_i is the boundary of the pre-image of an open sector M_{-i} containing the one of the cuts as in the proof of Theorem 5.2. We embed $M_+ = M \setminus M_{-1} \cup M_{-2}$ into the limit orbifold and pullback the complex structure, extending it to a complex structure J in M. As in Lemma 5.4, we have that the positive part of the limit after neck-stretching, M_+^∞, is symplectomorphic to the complement of the orbifold points in the limit orbifold.

Let us name $\alpha, \beta, \gamma, \varepsilon$ the classes of the Maslov index 2 holomorphic disks living in the complement of the orbifold points of the limit orbifold $\overline{M_+^\infty}$ [5, Corollary 6.4]. We consider a J-holomorphic disk u with boundary on $T_1(a,b)$, and we look at the

degenerate pseudo-holomorphic disk u_+^∞ in the limit orbifold $\overline{M_+^\infty}$, which can be shown to be the compactification of the top building of the neck-stretch limit using an argument analogous to Lemma 5.4.

We name $\mathcal{A}, \mathcal{B}, \mathcal{C}$, the pre-image of the edges of the limit orbifold whose symplectic area are respectively $3a^2 - ab$, $3b^2 - ab$, and 3. We keep calling $\mathcal{E}$ the class of limit of the exceptional curve in the limit orbifold. Say that α intersects $\mathcal{A}$, β intersects $\mathcal{B}$, γ intersects $\mathcal{C}$ and ε intersects $\mathcal{E}$.

Proposition 5.5 *We have that* $\mathcal{A}\cdot\mathcal{A} = \frac{a^2-b^2}{b^2} < 0$, $\mathcal{B}\cdot\mathcal{B} = \frac{b^2-a^2}{a^2} > 0$, $\mathcal{C}\cdot\mathcal{C} = \frac{1}{a^2b^2} > 0$, $\mathcal{E}\cdot\mathcal{E} = -1 < 0$.

Proof Let's look at the limit orbifold of the ATBD of $\mathbb{C}P^2$, i.e., before the blow up. Call $\hat{\mathcal{A}}$, $\hat{\mathcal{B}}$, $\hat{\mathcal{C}}$ the preimages of its moment polytope edges. Similar to the discussion prior to Claim 4.6, we see that the second homology of this orbifold has one generator H such that, $[\hat{\mathcal{A}}] = a^2H$, $[\hat{\mathcal{B}}] = b^2H$, $[\hat{\mathcal{C}}] = H$ and from Claim 4.7 we have that $H \cdot H = 1/a^2b^2$.

So we see that, after the blow up, the limit orbifold has second homology generated by $\mathcal{E}$ and $H = \mathcal{C}$ (here we use the inclusion of the second homology of an orbifold into its one point blowup). Moreover, $\mathcal{A} + \mathcal{E} = a^2H$ and $\mathcal{B} + \mathcal{E} = b^2H$. We already know that $\mathcal{E}\cdot\mathcal{E} = -1$ and $\mathcal{A}\cdot\mathcal{E} = 1$, since $\mathcal{E}$ is an exceptional divisor and $\mathcal{A}$ the proper transform of $\hat{\mathcal{A}}$. From $\mathcal{C}\cdot\mathcal{E} = 0$ we have that $\mathcal{A}\cdot H = 1/b^2$. Hence, $\mathcal{A}\cdot\mathcal{A} + 1 = a^2/b^2$ and the first equality of the Proposition follows. In a similar fashion we see that $\mathcal{B}\cdot\mathcal{B} = \frac{b^2-a^2}{a^2}$. □

Remark 5.6 One can prove the formula below:

$$\mathcal{D}\cdot\mathcal{D} = \frac{|\mathbf{w}\wedge\mathbf{v}|}{|\mathbf{v}\wedge\mathbf{u}||\mathbf{w}\wedge\mathbf{u}|},$$

where $\mathcal{D}$ is represented by an edge of the moment polytope of a toric orbifold, for which the corresponding primitive vector is $\mathbf{u}$, and such that the primitive vectors corresponding to the adjacent edges are $\mathbf{v}$ and $\mathbf{w}$, which both point towards the edge $\mathcal{D}$. This way $|\mathbf{w}\wedge\mathbf{u}||\mathbf{v}\wedge\mathbf{u}| > 0$. We also have that, if $\mathbf{u}\wedge\mathbf{n} > 0$, where $\mathbf{n}$ is normal to $\mathcal{D}$ and points inside the polytope, then $\mathbf{u}$ points from the $\mathbf{w}$-edge to the $\mathbf{v}$-edge.

When $|\mathbf{w}\wedge\mathbf{v}| > 0$, one can analyse intersections in the orbifold whose moment polytope is a triangle with edges $\mathbf{v}$, $\mathbf{u}$, $\mathbf{w}$. As in Claim 4.7, one have that the second homology of the orbifold has a generator H for which $\mathcal{D} = |\mathbf{w}\wedge\mathbf{v}|H$ and

$$H\cdot H = \frac{1}{|\mathbf{w}\wedge\mathbf{v}||\mathbf{v}\wedge\mathbf{u}||\mathbf{w}\wedge\mathbf{u}|}.$$

If $|\mathbf{w}\wedge\mathbf{v}| < 0$, one can look at the orbifold whose moment polytope is a quadrilateral with edges $\mathbf{v}$, $\mathbf{u}$, $\mathbf{w}$, $-\mathbf{u}$. The result follows from an analysis similar to the proof of Proposition 5.5. □

From Proposition 5.5, we see that the positivity of intersection argument given in the proof of Theorem 5.2 fails. Nonetheless we have:

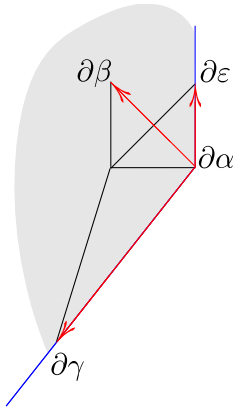

Fig. 26 $\partial\alpha$ is a corner of $\mho_{T_1(a,b)}$

Lemma 5.7 *The intersections* $\mathcal{E}\cdot[u_+^\infty]$, $\mathcal{B}\cdot[u_+^\infty]$ *and* $\mathcal{C}\cdot[u_+^\infty]$ *are non-negative.*

Proof That $\mathcal{C}\cdot[u_+^\infty]\geq 0$ and $\mathcal{B}\cdot[u_+^\infty]\geq 0$ follows as before, since a component of u_+^∞ contributing negatively to $\mathcal{C}\cdot[u_+^\infty]$ would have to be a positive multiple of $\mathcal{C}$, but $\mathcal{C}\cdot\mathcal{C}>0$. Similar for $\mathcal{B}$. In fact, no component could be a multiple of $\mathcal{B}$, since its area is $3b^2-ab>ab$ $(b>a)$, and the area of a Maslov index 2 disk is equal to the area ab of the Chern one sphere $\mathcal{E}$, by monotonicity.

That $\mathcal{E}\cdot[u_+^\infty]\geq 0$ follows from $\omega_+^\infty\cdot\mathcal{E}=\omega_+^\infty\cdot[u_+^\infty]=ab$. Since u_+^∞ has the 'main component' with boundary on (the limit of) $T_1(a,b)$, and all components have positive symplectic area, we can't have a multiple of $\mathcal{E}$. □

Lemma 5.8 *Upon identification of* $T_1(a,b)$ *with its limit in the limit orbifold, we have that* $\partial\alpha$ *is a corner of the boundary Maslov-2 convex hull* $\mho_{T_1(a,b)}$.

Proof First we notice that the count of J-holomorphic disks in the class α is ± 1, by the same arguments as in [37, Lemma 4.11]. So $\partial\alpha$ is in $\mho_{T_1(a,b)}$.

The classes of Maslov index 2 (or symplectic area ab) disks with boundary in (the limit of) $T_1(a,b)$ inside the limit orbifold must be of the form:

$$\alpha+k(\varepsilon-\alpha)+l(\beta-\alpha)+m(\gamma-\alpha). \tag{5.1}$$

Recall that $\alpha,\beta,\gamma,\varepsilon$ are Maslov index 2 classes.

By Lemma 5.7, we see that the class $[u_+^\infty]$ must have $k,l,m\in\mathbb{Z}_{\geq 0}$ in (5.1). Hence $\partial\alpha$ is a corner of $\mho_{T_1(a,b)}$, see Fig. 26. □

Lemma 5.9 *The affine angle of the corner* $\partial\alpha$ *in* $\mho_{T_1(a,b)}$, *i. e., the norm of the determinant of the primitive vectors of the edges of the corner, is* $b'=3a-b$.

Proof Up to a choice of signs, we may identify $\partial\alpha=(1,0)$, $\partial\beta=(0,1)$, $\partial\epsilon=(1,1)$, $\partial\gamma=(-a^2,-b^2)$ (see Fig. 7). Recall that $1+a^2=bb'$. Hence $\partial\gamma-\partial\alpha=-b(b',b)$. Therefore the primitive vectors are $(0,1)$ and (b',b). □

Lemma 5.10 *The Maslov-2 convex hull* $\mho_{T_1(a,b)}$ *is compact.*

Proof By area reasons, there is a constant $N_0 \in \mathbb{Z}_{>0}$ such that $[u_+^\infty]$ cannot have N_0 or more components in the class $\mathcal{A}$, for all pseudo-holomorphic disks u. Therefore, there is a constant $N \in \mathbb{Z}_{>0}$ such that $\mathcal{A} \cdot [u_+^\infty] > -N$. So, $k + l + m < N + 1$ in the decomposition (5.1) of $[u_+^\infty]$, which implies the Lemma. □

Recall that two Maslov-2 convex hull are equivalent if they are related via $SL(2, \mathbb{Z})$. Since we have an infinite number of values of affine angles, the number of equivalence classes for the Maslov-2 convex hulls $\mho_{T_1(a,b)}$s cannot be finite. Note that here we use Lemma 5.10, since if not compact, a Maslov-2 convex hull can have infinitely many corners. This finishes the proof of Theorem 1.1(b).

5.3 Proof of Theorem 1.6

Let (X, ω) be a del Pezzo surface and consider $\Theta_{p,q,r}^{n_1,n_2,n_3} \subset X$ the monotone Lagrangian tori described in this Sect. 5. Consider Σ the smooth anti-canonical divisor living over the boundary of the base of an ATF [31, Proposition 8.2] that has no elliptic rank one singularity [31, Definition 4.2], [35, Definition 2.7]. If one applies nodal slide along a segment $[P, Q]$ inside the base of an ATF, the new ATF can be chosen to be equal to the previous one outside a small neighbourhood of $[P, Q]$. By only sliding the nodes away from a neighbourhood $\mathcal{N}$ of Σ, we can assume that this neighbourhood remains invariant under the mutations of the ATBD's, so Σ is always living over the boundary of the base of corresponding ATF.

We can take $\mathcal{N}$ to be a normal disk bundle $p : \mathcal{N} \to \Sigma$ for which the symplectic area of the fibres is $\pi\epsilon^2$, for small ϵ. We assume that $\mathcal{N}$ is the pre-image of the fibres of the ATF which bound a Maslov index two disk of area $\pi\epsilon^2$ project to a segment in the ATF and intersecting each fibre in a collapsing cycle, see Fig. 27. By the symplectic neighbourhood theorem, we have that for $D = p^{-1}(x)$, $T_x X = T_x D \oplus (T_x D)^{\omega^\perp}$ where $(T_x D)^{\omega^\perp}$ is the symplectic orthogonal of $T_x D$. Moreover, up to a symplectomorphism, $\omega_{|\mathcal{N}} = r dr \wedge d\theta + \hat{\omega}$, where $\hat{\omega} = p^* \omega_{|\Sigma}$, $re^{i\theta}$ are coordinates on the disk fibre. Since Σ is anti-canonical, the first Chern class of its normal bundle is equal to the first Chern class of $TX_{|\Sigma}$, and by monotonicity, it is the class $K[\omega_{|\Sigma}]$, for some $K > 0$. Therefore, there is a one-form α on the $\mathbb{D}^*$-bundle $p : \mathcal{N} \setminus \Sigma \to \Sigma$, for which $d\alpha = K\hat{\omega}$. In other words, α is so that $(\partial\mathcal{N}, \alpha_{|\partial\mathcal{N}})$ is the pre-quantization of $(\Sigma, K\omega_{|\Sigma})$ (up

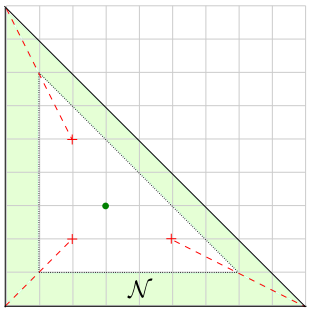

Fig. 27 The neighbourhood $\mathcal{N}$ of Σ is the pre-image of the shaded region

to a factor of $\pm 2\pi$ depending in one's definition). So we have $\omega_{|\mathcal{N}} = d\eta$, where $\eta = (r^2/2 - 1)d\theta + \hat{\alpha}$, $\hat{\alpha} = K^{-1}\alpha$ and $\eta_{|\partial\mathcal{N}}$ is a contact form in $\partial\mathcal{N}$.

Let $V = \partial(X \setminus \mathcal{N})$. In a neighbourhood of V, there is a Liouville vector field S pointing outside V for which the corresponding Reeb vector field $R \subset \Gamma(TV)$ is so that ${}^{V}/_{R} \cong \Sigma$. Indeed, take S so that $\iota_S\omega = \gamma$, since $\epsilon < \sqrt{2}$, we see that S points outside of V and R is a vector field that rotates the fibre of the S^1-bundle $p : \partial\mathcal{N} \to \Sigma$, hence $({}^{V}/_{R}, \hat{\omega}_{|V}) \cong (\Sigma, \omega_{|\Sigma})$.

We now attach the positive symplectization of V to $X \setminus \mathcal{N}$. Because V is foliated by Legendrian tori, which are fibres of the ATF, we can extend the ATF in $X \setminus \mathcal{N}$ to $(X \setminus \mathcal{N}) \cup (V \times [0, +\infty))$. So we can see $\Theta^{n_1,n_2,n_3}_{p,q,r} \subset (X \setminus \mathcal{N}) \cup (V \times [0, +\infty))$ as a fibre of an ATF, see Fig. 9. It follows from seeing $X \setminus \mathcal{N}$ coming from Weinstein handle attachments to the co-disk bundle $\mathbb{D}^*_{\leq \epsilon}\Theta^{n_1,n_2,n_3}_{p,q,r}$ along the boundary of Lagrangian disks, that $\Theta^{n_1,n_2,n_3}_{p,q,r}$ are exact in $(X \setminus \mathcal{N}) \cup (V \times [0, +\infty))$, see Sect. 6.1.

Theorem (1.6) *The tori* $\Theta^{n_1,n_2,n_3}_{p,q,r} \subset (X \setminus \mathcal{N}) \cup (V \times [0, +\infty))$ *belong to mutually different Hamiltonian isotopy classes.*

Proof If there were a Hamiltonian isotopy between two of these tori, it could be made to be the identity outside $(X \setminus \mathcal{N}) \cup (V \times [0, C))$, for some constant C. Therefore it is enough to prove that the tori are not Hamiltonian isotopic in the del Pezzo surface (X, ω_C), obtained by collapsing the Reeb vector field inside $V \times \{C\}$, see Fig. 9. In other words, (X, ω_C) is obtained by inflating X along Σ by a factor of C. We note that $\Sigma \subset X$ not only represents the Poincaré dual to c_1, but as a cycle in $X \setminus \Theta^{n_1,n_2,n_3}_{p,q,r}$, it represents the Poincaré dual to half of the Maslov class $\mu/2 \in H^2(X, \Theta^{n_1,n_2,n_3}_{p,q,r})$. Looking at the ATF in $(X \setminus \mathcal{N}) \cup (V \times [0, C))$ we see that, not only $\Theta^{n_1,n_2,n_3}_{p,q,r} \subset (X, \omega_C)$ remains monotone, it is the monotone fibre of an ATBD of (X, ω_C), which is the corresponding multiple of the initial ATBD of (X, ω), see Fig. 9. Hence the tori $\Theta^{n_1,n_2,n_3}_{p,q,r}$ are mutually non-Hamiltonian isotopic in (X, ω_C). □

Remark 5.11 Note that taking the complement of the divisor that is Poincaré dual to a multiple of the Maslov class for all tori was essential. All Lagrangian tori constructed in $\mathbb{C}P^2$ can be shown to live in the complement of a line. But Dimitroglou Rizell is working towards the classification of tori in $\mathbb{C}^2$ which aims to show that there are only Clifford and Chekanov monotone Lagrangian tori in $\mathbb{C}^2$, up to Hamiltonian isotopy (see [7]).

6 Relating to other works

6.1 Shende–Treumann–Williams

Consider a surface S and a closed circle $\sigma \subset S$. Let $M = D^*S$ the co-disk bundle of S (with respect to some auxiliary metric on S). We can lift σ to a Legendrian $\sigma' \subset \partial M$, by considering over each point $s \in \sigma$ the co-vector that vanishes on the tangent vectors of σ at s. We can then attach a Weinstein handle along σ' obtaining a new Liouville manifold M_σ. Shende-Treumann-Williams show that there is a way to "mutate" the surface S by sliding it along the Lagrangian core $L_{\sigma'}$ of the Weinstein handle, obtaining

a new exact Lagrangian S^σ. We also note that M_σ is homotopic equivalent to $S \cup L_\sigma$, where L_σ is a Lagrangian disk with boundary $\sigma \subset S$ given by the continuation of the Lagrangian core $L_{\sigma'}$ where we shrink the length of the co-vectors of σ' to zero.

This idea can be generalized for any number of cycles $\sigma_1, \ldots, \sigma_n$ in S, where we obtain a Liouville manifold $M_{\sigma_1,\ldots,\sigma_n}$, with a Lagrangian skeleton given by $S \cup L_{\sigma_1} \cdots \cup L_{\sigma_n}$, where L_{σ_i} is a Lagrangian disk with boundary on σ_i, see [30, Definitions 1.1, 1.2, 1.3]. Also, assuming that $\sigma_1, \ldots, \sigma_n$ form a non-degenerate configuration [30, Definition 1.13] for any word w on $\sigma_1, \ldots, \sigma_n$, one can obatain a surface S^w mutated along Lagrangian disks according to the word w. Moreover, Shende-Treumann-Williams show how to also mutate the Lagrangian disks, to obtain Lagrangians disks $L^w_{\sigma_i^w}$'s with boundary on S^w so that $M_{\sigma_1,\ldots,\sigma_n}$ has $S^w \cup L^w_{\sigma_1^w} \cdots \cup L^w_{\sigma_n^w}$ as a Lagrangian skeleton. In the case S is a torus T and $\sigma_i's$ geodesics, then they show that $\sigma_1, \ldots, \sigma_n$ form a non-degenerate configuration and how these mutations can be encoded using cluster algebras [30, Theorem 1.14].

Question 6.1 ([30] (Section 1.2.3)). Do the S^w's give infinitely many Hamiltonian isotopy classes of exact Lagrangians in $M_{\sigma_1,\ldots,\sigma_n}$?

When S is a torus T, this is precisely what is happening in the complement of the anti-canonical surface Σ living over the boundary of the base of the monotone ATFs. We claim (without giving a proof) that if the cycles σ_i's are taken to be periodic orbits of the self torus action of T, then we obtain an ATF on $M_{\sigma_1,\ldots,\sigma_n}$. Moreover, the ATF can be represented by an ATBD whose cuts point towards the image of T and are in the direction of the cycles σ via the identification of $H_1(T, \mathbb{R})$ with $\mathbb{R}^2 \supset$ ATBD. The Lagrangian disks live over the segment uniting the image of T in the ATBD with the nodes, see Fig. 28. In that way, the torus T^w mutated with respect to a word w on $\sigma_1, \ldots, \sigma_n$ corresponds to sliding the nodes over the central fibre according to w, see [30, Section 6], in particular Section 6.2. Also, if each time we slide a node through the central fibre we perform a mutation of the ATBD, the homology classes in $H_1(T, \mathbb{Z})$ of the boundaries of the mutated Lagrangian disks $L^w_{\sigma_i^w}$'s are identified with the primitive directions of the cuts of the mutated ATBD.

Figure 28 illustrates $\mathbb{C}P^2\#6\overline{\mathbb{C}P^2} \setminus \Sigma$, where we have nine Lagrangian disks living over the segments connecting the central fibre to each of the nodes of the ATBD.

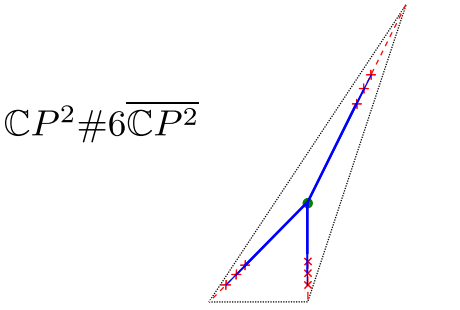

Fig. 28 The complement of an anti-canonical surface in $\mathbb{C}P^2\#6\overline{\mathbb{C}P^2}$ as a result of attaching nine Lagrangian disks to the central fibre

Theorem 1.6 shows that total mutations give rise to tori $\Theta^{3,3,3}_{p,q,r}$ living in mutually distinct Hamiltonian isotopy classes.

6.2 Keating

In [18, Proposition 5.21], Keating shows how the Milnor fibres

$$\mathcal{T}_{3,3,3} = \{x^3 + y^3 + z^3 + 1 = 0\};$$
$$\mathcal{T}_{2,4,4} = \{x^2 + y^4 + z^4 + 1 = 0\};$$
$$\mathcal{T}_{2,3,6} = \{x^2 + y^3 + z^6 + 1 = 0\};$$

compactify respectively to the del Pezzo surfaces $\mathbb{C}P^2\#6\overline{\mathbb{C}P^2}$, $\mathbb{C}P^2\#7\overline{\mathbb{C}P^2}$, $\mathbb{C}P^2\#8\overline{\mathbb{C}P^2}$.

Also, in [17, Section 7.4], Keating describes how the Milnor fibres $\mathcal{T}_{p,q,r}$ of $x^p + y^q + z^r + axyz$ can be obtained by attaching p, q, r Weinstein handles to D^*T along Legendrian lifts of three circles, mutually intersecting at one point. By our discussion on the precious section, we see the compactifications described in [18, Proposition 5.21] depicted in Figs. 19(B_2), 20(B_2), 21(C_2).

The standard symplectic form on the Milnor fibres is the one obtained after completion, i.e., by attaching the positive part of the symplectization of its boundary, as we considered in Sect. 5.3. As a consequence of Theorem 1.6, we have that there are infinitely many exact Lagrangian tori in $\mathcal{T}_{3,3,3}, \mathcal{T}_{2,4,4}, \mathcal{T}_{2,3,6}$.

6.3 Karpov–Nogin and Hacking–Prokhorov

There seems to be a relation between complete m-block collections of sheaves [20] on a del Pezzo surface and its ATBDs. By the Theorem in [20, Section 3], a complete 3-block collection on a degree d del Pezzo suface containing exceptional collections with n_1,n_2,n_3 sheaves of ranks p, q, r, satisfy the Markov type one equation (2.1).

Question 6.2 Suppose we have an ATBD with node type $((n_1, p_1), \ldots, (n_m, p_m))$ of a del Pezzo surface. Is there a complete m-block collection $(\mathcal{E}_1, \ldots, \mathcal{E}_m)$, so that the exceptional collection $\mathcal{E}_i$ contains n_i sheaves of rank p_i?

There is also a relation between $\mathbb{Q}$-Gorenstein smoothing [16] and ATBD on the smooth surface. In [16, Theorem 1.2], it is shown that the weighted projective planes that admit a $\mathbb{Q}$-Gorenstein smoothing are precisely the ones given by the limit orbifolds of the ATBDs obtained by total mutation of the ones in Fig. 1. It seems that pushing the nodes towards the edges of an ATBD corresponds to degenerating the del Pezzo surface to the limit orbifold.

Question 6.3 Do monotone Lagrangians of a del Pezzo know about its degenerations? In other words, does the limit orbifold of an ATBD have a $\mathbb{Q}$-Gorenstein smoothing to the corresponding del Pezzo?

6.4 FOOO and Wu

The singular fibration of $\mathbb{C}P^1 \times \mathbb{C}P^1$ described in [13] can be thought of as being a degeneration of the ATBD (A_3) of Fig. 22 where both nodes approach the edge, but instead of degenerating to an orbifold point, a Lagrangian sphere that lives between the nodes survive. Similarly, the ATBD of $\mathbb{C}P^2$ with limit orbifold $\mathbb{C}P(1, 1, 4)$, can be thought to "degenerate" to the singular fibration described in [38], where instead of an orbifold point we have a Lagrangian $\mathbb{R}P^2$ (which is a Lagrangian pinwheel $L_{1,2}$ [10, Definitions 2.1, 2.3] [19, Definition 3.1], seen as a visible surface of the cut of an ATBD of $\mathbb{C}P^2$ with limit orbifold $\mathbb{C}P(1, 1, 4)$ [10, Remark 2.6]). Indeed, $\mathbb{C}P^1 \times \mathbb{C}P^1$ can be obtained as a symplectic cut [38, Section 3] from T^*S^2 and $\mathbb{C}P^2$ as a symplectic cut from $T^*\mathbb{R}P^2$. In fact, there is a two-to-one cover $\mathbb{C}P^1 \times \mathbb{C}P^1 \to \mathbb{C}P^2$ branched over a conic, which extend the standard two-to-one cover $T^*S^2 \to T^*\mathbb{R}P^2$. We refer the reader to [38, Sections 3.1, 3.2], for a detailed description of these singular fibrations.

The point is: in [13] it is shown that there is a continuum of non-displaceable fibres of the singular fibration described. It follows that there is a continuum of non-displaceable fibres on the ATBD (A_3) of Fig. 22. By [36, Theorem 1.8] (see also [36, Section 7]), we also have of non-displaceable fibres on the ATBD (A_3) of $\mathbb{C}P^2\#3\overline{\mathbb{C}P^2}$ depicted in Fig. 16. The non-displaceability of the analogous fibres for the $\mathbb{C}P^2$ case is an open question. In [36], a similar result is also proven for some family of tori in the monotone $(\mathbb{C}P^1)^{2m}$.

Question 6.4 Which of the ATBDs described in this paper have a continuum of non-displaceable fibres?

Acknowledgements We would like to thank Ivan Smith, Dmitry Tonkonog, Georgios Dimitroglou Rizell, Denis Auroux, Jonathan David Evans, Harold Williams and Kaoru Ono for useful conversations. The exposition of the paper was greatly improved by the comments of an anonymous referee. Section 6 was very much motivated by talks given by Vivek Shende and Ailsa Keating at the Symplectic Geometry and Topology Workshop held in Uppsala on September 2015.

References

1. Auroux, D.: Mirror symmetry and T-duality in the complement of an anticanonical divisor. J. Gökova Geom. Topol. **1**, 51–91 (2007)
2. Auroux, D.: Special Lagrangian fibrations, wall-crossing, and mirror symmetry. In: Cao, H.-D., Yau, S.-T. (eds.) Surveys in Differential Geometry. Vol. XIII. Geometry, Analysis, and Algebraic Geometry: Forty Years of the Journal of Differential Geometry, Volume 13 of Surveys in Differential Geometry, pp. 1–47. International Press, Somerville (2009)
3. Bourgeois, F., Eliashberg, Y., Hofer, H., Wysocki, K., Zehnder, E.: Compactness results in symplectic field theory. Geom. Topol. **7**, 799–888 (2003)
4. Chen, W.: Orbifold adjunction formula and symplectic cobordisms between lens spaces. Geom. Topol. **8**, 701–734 (2004). (electronic)
5. Cho, C.H., Poddar, M.: Holomorphic orbi-discs and Lagrangian Floer cohomology of symplectic toric orbifolds. J. Differ. Geom. **98**(1), 21–116 (2014)

6. Chen, W., Ruan, Y.: Orbifold Gromov–Witten theory. In: Adem, A., Morava, J., Ruan, Y. (eds.) Orbifolds in Mathematics and Physics (Madison, WI, 2001), Volume 310 of Contemporary Mathematics, pp. 25–85. American Mathematical Society, Providence (2002)
7. Dimitroglou Rizell, G., Goodman, E., Ivrii, A.: Lagrangian isotopy of tori in $S^2 \times S^2$ and $\mathbb{C}P^2$. arXiv:1602.08821 (2016)
8. Eliashberg, Y., Givental, A., Hofer, H.: Introduction to symplectic field theory. Geom. Funct. Anal. (Special Volume, Part II), pp. 560–673, 2000. GAFA 2000 (Tel Aviv, 1999)
9. Eliashberg, Y., Polterovich, L.: Unknottedness of Lagrangian surfaces in symplectic 4-manifolds. Int. Math. Res. Not. **11**, 295–301 (1993)
10. Evans, J.D., Smith, I.: Markov numbers and Lagrangian cell complexes in the complex projective plane. arXiv:1606.08656v2 (2016)
11. Fukaya, K., Oh, Y.-G., Ohta, H., Ono, K.: Lagrangian Intersection Floer Theory: Anomaly and Obstruction, Volume 46 of Studies in Advanced Mathematics. American Mathematical Society, International Press, Somerville (2010)
12. Fukaya, K., Oh, Y.-G., Ohta, H., Ono, K.: Lagrangian Floer theory on compact toric manifolds II: bulk deformations. Sel. Math. (New Ser.) **17**(2), 609–711 (2011)
13. Fukaya, K., Oh, Y.-G., Ohta, H., Ono, K.: Toric degeneration and nondisplaceable Lagrangian tori in $S^2 \times S^2$. Int. Math. Res. Not. **13**, 2942–2993 (2012)
14. Gromov, M.: Pseudo holomorphic curves in symplectic manifolds. Invent. Math. **82**, 307–347 (1985)
15. Galkin, S., Usnich, A.: Laurent phenomenon for Landau–Ginzburg potential. http://research.ipmu.jp/ipmu/sysimg/ipmu/417.pdf (2010)
16. Hacking, P., Prokhorov, Y.: Smoothable del Pezzo surfaces with quotient singularities. Compos. Math. **146**(1), 169–192 (2010)
17. Keating, A.: Homological mirror symmetry for hypersurface cusp singularities. arXiv:1510.08911 (2015)
18. Keating, A.: Lagrangian tori in four-dimensional Milnor fibres. Geom. Funct. Anal. **25**(6), 1822–1901 (2015)
19. Khodorovskiy, T.: Symplectic rational blow-up. arXiv:1303.2581 (2013)
20. Karpov, B.V., Nogin, D.Y.: Three-block exceptional sets on del Pezzo surfaces. Izv. Ross. Akad. Nauk Ser. Mat. **62**(3), 3–38 (1998)
21. Li, T.J., Liu, A.: Symplectic structure on ruled surfaces and a generalized adjunction formula. Math. Res. Lett. **2**(4), 453–471 (1995)
22. Lalonde, F., McDuff, D.: The classification of ruled symplectic 4-manifolds. Math. Res. Lett. **3**(6), 769–778 (1996)
23. Leung, N.C., Symington, M.: Almost toric symplectic four-manifolds. J. Symplectic Geom. **8**(2), 143–187 (2010)
24. McDuff, D.: The structure of rational and ruled symplectic 4-manifolds. J. Am. Math. Soc. **3**(3), 679–712 (1990)
25. McDuff, D.: From symplectic deformation to isotopy. In: Topics in Symplectic 4-manifolds (Irvine, CA, 1996), First International Press Lecture Series, I, pp. 85–99. International Press, Cambridge (1998)
26. McDuff, D., Salamon, D.A.: Introduction to Symplectic Topology. Oxford Mathematical Monographs. The Clarendon Press Oxford University Press, Oxford (1998)
27. Ohta, H., Ono, K.: Notes on symplectic 4-manifolds with $b_2^+ = 1$. II. Int. J. Math. **7**(6), 755–770 (1996)
28. Ohta, H., Ono, K.: Symplectic 4-manifolds with $b_2^+ = 1$. In: Andersen, J.E., Dupont, J., Pedersen, H., Swann, A. (eds.) Geometry and Physics (Aarhus, 1995), Volume 184 of Lecture Notes in Pure and Applied Mathematics, pp. 237–244. Dekker, New York (1997)
29. Salamon, D.: Uniqueness of symplectic structures. Acta Math. Vietnam. **38**(1), 123–144 (2013)
30. Shende, V., Treumann, D., Williams, H.: On the combinatorics of exact Lagrangian surfaces. arXiv:1603.07449v1
31. Symington, M.: Four dimensions from two in symplectic topology. In: Topology and Geometry of Manifolds (Athens, GA, 2001), Volume 71 of Proceedings of Symposia in Pure Mathematics, pp. 153–208. American Mathematics Society, Providence (2003)
32. Taubes, C.H.: The Seiberg–Witten and Gromov invariants. Math. Res. Lett. **2**(2), 221–238 (1995)
33. Taubes, C.H.: SW $\Rightarrow$ Gr: from the Seiberg–Witten equations to pseudo-holomorphic curves. J. Am. Math. Soc. **9**(3), 845–918 (1996)

34. Taubes, C.H.: Seiberg Witten and Gromov Invariants for Symplectic 4-Manifolds, Volume 2 of First International Press Lecture Series. Wentworth, R. (ed.) International Press, Somerville (2000)
35. Vianna, R.: On exotic Lagrangian tori in $\mathbb{CP}^2$. Geom. Topol. **18**(4), 2419–2476 (2014)
36. Vianna, R.: Continuum families of non-displaceable Lagrangian tori in $(\mathbb{C}P^1)^{2m}$. arXiv:1603.02006 (2016)
37. Vianna, R.: Infinitely many exotic monotone Lagrangian tori in $\mathbb{CP}^2$. J. Topol. **9**(2), 535–551 (2016)
38. Wu, W.: On an exotic Lagrangian torus in $\mathbb{C}P^2$. Compos. Math. **151**(7), 1372–1394 (2015)
39. Zung, N.T.: Symplectic topology of integrable Hamiltonian systems. II. Topological classification. Compos. Math. **138**(2), 125–156 (2003)